Sepsis-trained macrophages promote antitumoral tissue-resident T cells

Alexis Broquet, Victor Gourain, Thomas Goronflot, Virginie Le Mabecque, Debajyoti Sinha, Mitra Ashayeripanah, Cédric Jacqueline, Pierre Martin, Marion Davieau, Lea Boutin, et al.

Title: Sepsis-trained macrophages promote anti-tumoral tissue-resident T cells

Authors: Alexis Broquet[1,2#], Victor Gourain[1#], Thomas Goronflot[3#], Virginie Le Mabecque[1], Debajyoti Sinha[1] , Mitra Ashayeripanah[4], Cédric Jacqueline[1], Cecile Poulain[1,2], Florian P. Martin[1,2], Cynthia Fourgeux[1], Manon Cannevet[2], Thomas Leclercq[1], Maeva Guilonneau[1], Tanguy Chaumette[1], Thomas Laurent[1], Christelle Harly[5], Emmanuel Scotet[5], Laurent Legentil[6], Vincent Ferrières[6], Stephanie Corgnac[7], Fathia Mami-Chouaib[7], Jean Francois Mosnier[8], Nicolas Mauduit[9], Hamish E.G. McWilliam[4], Jose A. Villadangos[4,10], Pierre Antoine Gourraud[1,3], Karim Asehnoune[1,2], Jeremie Poschmann[1]* and Antoine Roquilly[1,2,4]*

Affiliations:

[1]Nantes Université, CHU Nantes, INSERM, Center for Research in Transplantation and Translational Immunology, UMR 1064; F-44000, Nantes, France.

[2] CHU Nantes, INSERM, Nantes Université, Anesthesie Reanimation, CIC 1413; F-44000 Nantes, France.

[3] Nantes Université, CHU Nantes, Pôle Hospitalo-Universitaire 11 : Santé Publique, Clinique des données, INSERM, CIC 1413; F-44000 Nantes, France.

[4] Department of Microbiology and Immunology, The University of Melbourne, The Peter Doherty Institute for Infection and Immunity; Melbourne, Victoria 3000, Australia.

[5] Nantes Université, INSERM, CRC2INA, Nantes, France.

[6] Univ Rennes, Ecole Nationale Supérieure de Chimie de Rennes, CNRS, ISCR – UMR 6226; F-35000 Rennes, France.

[7] INSERM UMR 1186, Integrative Tumour Immunology and Immunotherapy, Gustave Roussy, Fac. de Médecine—Univ. Paris-Sud, Université Paris-Saclay; Villejuif, France.

[8] CHU Nantes, Nantes Université, Anatomo-pathologie; F-44000 Nantes, France.

[9] Nantes Université, CHU Nantes, PMSI; Nantes, France.

[10] Department of Biochemistry and Pharmacology, Bio21 Molecular Science and Biotechnology Institute, The University of Melbourne; Parkville, Victoria 3010, Australia.

*Corresponding authors.

Antoine Roquilly. 20 bvd Benoni Goullin, 44000 Nantes, France. Ph: +33 253482230 e-mail: antoine.roquilly@univ-nantes.fr

Jeremie Poschmann. 30 boulevard Jean-Monnet, 44093 Nantes, France. Ph: +33240087899 e-mail: jeremie.poschmann@univ-nantes.fr

[#] These authors contributed equally to this work.

[*] These authors jointly directed this work.

Abstract: Sepsis induces immune alterations which last for months after the cure. The impact of this immunological reprogramming on the long-term risk of cancer remains unclear. Using a national registry, we observed that sepsis survivors had a lower cumulative incidence of cancers than matched controls. We identified the $CXCR6^+$ tissue-resident T cells, mainly composed of $IL17^+$ $ROR\gamma t^+$ $V\gamma 6\delta$ T cells, as cells responsible for this decreased tumoral growth after sepsis. We then identified a chemokine network released from sepsis-trained macrophages that triggers tissue residency of T cells via CXCR6 and CCR2 stimulation. The injection of laminarin could therapeutically reproduce this protective sepsis consequence. High Cxcr6/Ccr2 gene co-expression is associated with prolonged survival in lung adenocarcinoma patients.

One-Sentence Summary: Prolonged immune reprogramming decreases the risk of developing cancer in patients cured of sepsis

Main Text:

Infections are one of the most frequent causes of death worldwide (*1*), and their reported incidence increased even before the SARS-CoV2 pandemic (*2*). Sepsis, defined as life-threatening organ dysfunction caused by a dysregulated host response to infection (*3*), is responsible for most infection-related deaths. This dysregulated host response belongs to the systemic inflammatory response syndrome (SIRS), which is characteristic of an excessive release of inflammatory cytokines that activate innate and acquired immunity (*4*). Of note, SIRS can also be caused by non-septic conditions such as severe trauma or major surgery (*5*). With improvement in its early recognition and adequate medical management, the risk of sepsis-related death has steadily decreased over the last decades. Thus, the number of patients living with potential long-term sequels after sepsis is augmented, with increased long-term risks of cardiovascular diseases and dementia (*6–8*).

Sepsis induces profound immune system modifications with either increased immune tolerance or trained innate immunity (*9–12*). We and others have demonstrated that the immune reprogramming observed after sepsis lasts for months (*13–15*). It is well established that chronic inflammation increases the risk of cancer (*16*); however, the effects of immune reprogramming in patients cured of sepsis on tumoral immune surveillance have not been thoroughly investigated.

We hypothesized that the risk of developing cancer could be altered by the immune reprogramming observed in sepsis survivors. First, we tested this hypothesis in real-world medical records from the

French national administrative health claims data on hospitalization and observed that human sepsis survivors had a lower global risk of developing cancer up to ten years after the cure. Hence, studying the immune reprogramming after sepsis may reveal mechanistic features governing immune tolerance or cancer control. By applying single-cell RNA sequencing in sepsis-cured mice, which showed reduced orthotopic lung cancer growth, we discovered a plausible mechanism mediated via trained alveolar macrophages increasing tissue residency of $CXCR6^+$ T cells, mainly composed of $IL17^+$ $ROR\gamma t^+$ $V\gamma 6\delta$ T cells. Our results notably showed that CCR2 stimulation during sepsis increased the expression of CXCR6 by T cells, making them suitable for tissue retention by $CXCL16^+$ trained alveolar macrophages. Our results comprehensively describe the long-term impact of sepsis on immunity and reveal the capacity of resident macrophages to regulate the residency of T cells, which act as a critical mediator of tumor immune surveillance. Our study identifies a novel and therapeutically relevant anti-tumor consequence of sepsis-induced trained immunity.

RESULTS

Decreased risk of cancer for up to ten years in sepsis survivors.

To investigate the impact of sepsis-induced prolonged immune alterations, we aimed to compare cancer risk in humans who have survived sepsis with the relevant-matched controls. For this, we used the French national insurance and administrative databases systems (French abbreviation SNDS) that gather codes for all claims data on private and public hospitalizations to compare cancer development after sepsis in patients hospitalized between January 2010 and December 2016, with an end follow-up in December 2020. French hospital activity is exhaustively included in the SNDS database as a comprehensive recording of all hospitalized patients nationwide. There were 5,856,479 adults who were hospitalized in France for severe trauma, acute brain injury, or pneumonia (**Figure 1A**). We excluded adults who had a medical history of cancer (n=883,687) or autoimmune disorder (n=384,744), died within 6 months of the index admission (n=237,702), had missing sociological data (n=64,296) or had several episodes of ICU hospitalization (n=474,838). We finally defined two groups to investigate the effects of sepsis (cohort 1; n=681,603) and non-septic SIRS (cohort 2; n=3,219,609) on cancer risk. We included patients with sepsis (infection and hospitalized in intensive care units for life-threatening conditions) or infection (infection and hospitalized in general wards without acute organ failure) in cohort 1; and patients with non-septic SIRS (hospitalized for severe trauma or brain injury, no infection and hospitalized in intensive care units for life-threatening conditions) and no-SIRS (hospitalized in a general ward, no infection or acute organ failure during

the hospitalization) in cohort 2 (**Figure 1A**). We were thus able to study the effect on the risks of cancer (total and by cause) up to ten years following discharge from hospitalization between sepsis vs. infection survivors (Sepsis effect) and between non-septic systemic inflammatory response syndrome (SIRS) and no-SIRS survivors (SIRS effect). The demographic description of the cohorts is reported in **Table S1**.

Ten years after discharge from index admission, the cumulative risk of cancer was lower in sepsis-survivors compared to infection-survivors (Relative Risk 0.93, 95%CI 0.91 to 0.95; p<0.0001, **Figure S1A**). To substantially reduce the biases associated with observational studies, we considered differences in patients' demographic (age, sex, obesity, alcoholism, cause of admission), social (coded area of residency), and environmental (coded hospital localization) risk factors of cancer between groups by individual matching in a 1:1 ratio sepsis-survivors with patients cured from infection. Results of the 1:1 matched approach are reported in Table S2. In the 1:1 matched comparison, the cumulative incidence of cancer remained lower in sepsis-survivors compared to infection-survivors (Relative Risk 0.90, 95%CI 0.87 to 0.93; p<0.001, **Figure 1B**). As estimated by the instantaneous relative risk of cancer, the effect of sepsis on the risk of developing cancer was constant over the five first years of follow-up (**Figure 1C** and **S1B** for results in the matched population samples). We observed that the effects of sepsis were not cancer-specific by estimating the relative risks of the ten most frequent sites of cancer (**Figure 1D**).

We questioned if the protective effect of severe acute inflammation was specific to sepsis or if it could be observed after non-septic SIRS as in cohort 2. Of note, patients of cohort 2 were approximatively ten years younger than those of cohort 1, and the rates of major cancer risk factors (obesity and alcoholism) were lower by almost 10% (**Tables S1 and S2**), thus precluding any comparison of the incidence of cancer between the two cohorts. Contrary to sepsis, non-septic SIRS was associated with an increased cancer incidence after ten years of follow-up (Relative Risk in the matched sample 1.21, 95%CI 1.17 to 1.26; p<0.0001; **Figure S1C-D** for results in the crude and matched populations). This effect remained constant over the study period (**Figure 1C**) and was not cancer-specific (**Figure 1D).** These data reinforced our hypothesis of a life-long immunological reprogramming after sepsis and suggested differences between sepsis and non-septic SIRS.

Sepsis-cured mice control lung cancer numbers, size, and growth

Despite the matching strategy, which limited the risk of bias for imbalanced personal, social, and environmental risk factors of cancer, other uncontrolled confounding factors could still be accounted for the observed reduction of the risk of cancer after sepsis. We thus aimed to test the impact of sepsis on the susceptibility to cancer in a controlled mice model. We took advantage of a model of non-lethal *Escherichia coli* (*E. coli*) pneumonia that recapitulates the human response to sepsis, including initial lung neutrophil recruitment and weight loss, followed by prolonged functional reprogramming of mononuclear phagocytes (*13*, *15*). We investigated the susceptibility of sepsis-cured mice to orthotopic Lewis lung carcinoma (LLC) (**Figure 2A**). While mice are considered cured of sepsis as of day 7, we observed that the development of LLC was decreased when injected 28 days after sepsis. More precisely, a decrease in the absolute number of tumors and tumor size was observed in sepsis-cured animals (**Figure 2A**). These macro-phenotypic alterations of tumor growth even four weeks after the curation of sepsis suggest a long-term reorganization of the lung immune system.

Single-cell RNA-seq of lung immune populations along with respiratory sepsis progression and cure.

Thus, we profiled the single-cell immune landscape throughout lung sepsis to identify the molecular and cellular alterations contributing to the reduced cancer development after sepsis. For this, we collected the lungs of uninfected mouse as well as 1-, 3- and 7-days post-infection which respectively represent the phase prior to infection (Day 0), the acute phase of sepsis (Day 1- Day 3), and the sepsis-cured state (Day 7). Lung tissue was dissociated, and immune cells were enriched using CD45 marker-based sorting (**Figure S2A**). To avoid batch effects due to experimental variations between single-cell experiments, all-time points were collected on the same day, labeled with hashtag antibodies to identify each time point, and processed in a single cell RNA-sequencing (s.c. RNA-seq) experiment. Our analysis included 10,542 cells after quality control, hashtag demultiplexing, and doublet removal, sampled from two independent experiments with two mice at each time point (see methods for processing, quality control, and doublet removal) (**Figure S2B**). We manually annotated cell clusters based on the most differentially expressed genes (**Figure S2C**). Annotation of these clusters revealed the presence of multiple subtypes of lymphocytes (T cells, B cells, and natural killer cells), innate immune cells (macrophages, monocyte-derived cells, and dendritic cells) as well as neutrophils (**Figure 2B)**. We observed a rapid reorganization of immune cell populations in the lungs as early as day 1. Immune alterations

during *E. coli* pneumonia (day 1 and day 3) included a notable increase in the frequency of neutrophils as expected during sepsis (**Figure 2C**). The most noticeable change in the immune compartment in the sepsis-cured condition (D7) was observed among T cells, specifically with the appearance of Cxcr6^{+} T cells (expressing Cxcr6, CD3g, Il-17 among the top five genes) (**Figure 2C-D and Figure S2C**). We confirmed by flow cytometry the increased number of CXCR6^{+} T cells in the lungs of sepsis-cured mice (**Figure 2E**) and observed that it lasted up to 56 days despite a progressive decrease (**Figure 2F**). Significantly, the numbers of CXCR6^{-} T cells changed little, suggesting a CXCR6-dependent accumulation of T cells after sepsis.

Local accumulation of CXCR6^{+} tissue-resident T cells after sepsis decreases cancer development

CXCR6 is a marker of tissue-resident T cells (*17*, *18*), known for their ability to mediate cytotoxic and cytokinin responses and increase immune control of cancer (*19*). We confirmed that accumulated CXCR6^{+} T cells of sepsis-cured mice had high membrane expressions of CD103 (Itgae), CD69, and CD44 (**Figure 2G**) and low gene expressions of Ccr7 and S1pr1 (**Figure S3**), which represent a canonical signature of tissue-resident T cells (*18*). To validate that CXCR6^{+} T cells are derived from tissue precursors, we labeled *in vivo* circulating immune cells by intravenous injections of PE^{+} anti-CD45 antibody. We observed that ~15% of CXCR6^{-} T cells were recruited from the blood to the lungs during sepsis, but CXCR6^{+} T cells remained PE^{-} confirming that these cells derived from local progenitors rather than being recruited via the bloodstream (**Figure 2H**). We thus hypothesized that the reduced cancer growth observed after sepsis was mediated by CXCR6-dependent accumulation of tissue resident T cells. Supporting a role for CXCR6, we observed that the number of tissue-resident T cells was lower after sepsis in Cxcr6 deficient mice than in wild-type mice (**Figure 2I**). We also noticed that sepsis increased the number of tissue resident T cells during LLC development but not in Cxcr6 deficient mice (**Figure 2J**) and that LLC growth was not reduced after sepsis in Cxcr6 deficient mice (**Figure 2K).** This series of experiments demonstrate that the resistance to cancer growth observed after sepsis curation is mediated by a CXCR6-dependant accumulation of tissue-resident T cells.

Accumulation of CXCR6^{+} tissue-resident T cells is specific to sepsis, but not *E. coli* infection nor to lungs

To determine whether the observed accumulation of CXCR6$^+$ T cells was specific to *E. coli*-induced sepsis or the lungs, we next analyzed T cell numbers and CXCR6 expression in two other models of lung inflammation: cocci gram-positive (*Staphylococcus aureus*) sepsis and aseptic systemic inflammatory response (traumatic brain injury). While we observed a lung accumulation of CXCR6$^+$ T cells seven days after *Staphylococcus aureus* pneumonia (**Figure S4A**), we did not observe changes in the CXCR6$^+$ T cell lung compartment in response to traumatic brain injury (**Figure S4B**). We also applied a systemic sepsis-like mice model (iv. injection of the TLR9 agonist CpG, which is a mimic of bacterial DNA)(*20*) to test the impact of sepsis on other organs. In this CpG systemic sepsis model, we observed an increase in the number and percentage of CXCR6$^+$ T cells in the bone marrow and a significant increase in the expression of CXCR6 by T cells not only in the bone marrow but also in the gut and spleen seven days after the injection (**Figure S4C**). The accumulation of CXCR6$^+$ T cells thus appears specific to sepsis and can be detectable in various organs.

CXCR6+ tissue-resident T cells are mainly composed of IL17$^+$ Vγ6δ T cells after sepsis

We further characterized these CXCR6$^+$ tissue-resident T cells and observed that ~ 50% were CD8$^+$ in uninfected mice, while in sepsis-cured mice, the majority belonged to γδ T cells (**Figure 3A and Figure S4D)**. We also observed that the CXCR6+ γδ T cells, equally distributed between Vγ1, Vγ 4, and Vγ6 chains (Heilig and Tonegawa nomenclature) in uninfected mice, were predominantly composed of IL-17$^+$ RORγt$^+$ Vγ6δ T cells in sepsis-cured mice (**Figure 3B-D**).

We also investigated by single-cell TCR sequencing (scTCR-seq) the impact of sepsis on the TCR-β repertoire of CXCR6$^+$ conventional T cells. We observed that the most frequent clonotypes were found in CXCR6$^+$ T cells of sepsis-cured mice (**Figure 3E-F**). We concluded that sepsis induces an oligoclonal expansion of CXCR6$^+$ tissue-resident CD4 and CD8 T cells and then questioned if this TCR selection modulated their functions. To address this question, we compared the transcriptomic signature of the clonally selected (most frequent clonotypes expressed by at least 4 cells) with non-clonally selected CXCR6+ tissue-resident T cells (clonotypes observed in only one cell) cells (**Figure 3G**). This approach found only nine differentially expressed genes (DEG), six directly associated with TCR, between clonally selected and non-selected T cells, suggesting that the direct recognition of the pathogen did not impact the functional properties of tissue resident conventional T cells after sepsis. We also aimed to investigate the impacts of sepsis

on the production of IFNγ by clonally selected T cells. To do so, we induced the formation of OVA-specific CD8 tissue-resident memory T cells in CD45.1$^+$ mice by injecting ovalbumin (intratracheal) and CD45.2$^+$ OVA-specific OT-I cells (intravenous). Two weeks after the induction of OVA-specific tissue-resident CD8 T cells, we induced *E. coli* pneumonia in mice, and seven days later, we analyzed *in vivo* the immune response to intratracheal OVA challenge (**Figure 3H**). We observed that sepsis increased the number of the preexisting OVA-specific CD8 tissue-resident T cells but did not alter the production of IFNγ in response to OVA stimulation (**Figure 3H**). Finally, we questioned if CXCR6 depletion affects the number of CD4, CD8, and γδ tissue resident T cells after sepsis and found that the deletion of CXCR6 decreased the number of tissue-resident γδ T cells but not of tissue-resident conventional CD4 or CD8 T cells (**Figure 3I**). This observation correlated with the level of CXCR6 expression on these cell subsets (**Figure S4E**). From this series of experiments, we concluded that the effect of sepsis on tumor growth was mainly independent of a prolonged modulation of the TCR signaling but rather caused by the increase in the number of CXCR6$^+$ tissue-resident T cells, mainly composed of IL-17$^+$ RORγt$^+$ Vγ6δ T cells.

Sepsis induces a local cytokine and chemokine network that decreases T cells tissue egress

We thus aimed at deciphering the role of the mediators of the lung microenvironment, TCR-independent, involved in the accumulation of tissue-resident CXCR6$^+$ T cells after sepsis. Identifying receptor-ligand (R-L) pairs from single-cell transcriptomics maps is a powerful tool for revealing central signaling mechanisms shaping cell fate (*21*, *22*). We selected the 15 receptors with the highest gene expression in the CXCR6$^+$ T cell cluster of the sc-RNAseq analysis (**Figure 2B**), then performed literature-based research to find their known ligands, and finally evaluated if these ligands were expressed in any immune cells (**Figure 4A).** To expand this bibliographic analysis to all potential R-L interactions in available datasets, we bioinformatically filtered all R expressed in the CXCR6$^+$ T cell cluster and associated each ligand with its expression profile across all cells and the sepsis time points to create R-L maps during (Day 3) and after sepsis (Day 7). We selected L-R pairs based on their correlation of expression, resulting in a graphical representation of inter-cellular L-R communications (**Figures 4B-C**). During sepsis (day 3), this unsupervised approach defined the CXCR6-Cxcl16 pairs (ligands mainly expressed by macrophages and dendritic cells) and IFNγR1-IFNγ (ligands mainly expressed by NK cells) pair and CCR2-Ccl2/Ccl6/Ccl7/Ccl8 pairs (all ligands expressed by macrophages). After the sepsis

cure (day 7), we found five additional pairs, including the TGFβRII-TGFβ1/Gdf15 (ligands mainly expressed by macrophages and dendritic cells) (**Figure 4B**).

We next aimed to functionally confirm the role of these L-R pairs in establishing tissue residency of T cells after sepsis. To prioritize exploring L-R pairs specific to CXCR6 T cells, we compared intracellular chemokine signaling gene expression between the five T cell clusters defined in the single-cell RNA-seq (**Figures S5-6**). While TGFβ imprinting was shown to reduce the functional plasticity and increase the longevity of tissue-resident T cell populations in resting conditions (*23*), we observed that its signaling was activated in the CXCR6^{+} T cell cluster to a similar extent to other T cells, suggesting no specific role of TGF-β after sepsis (**Figure S6**). While we selected the IfnγR1-Ifnγ pair, the interferon type II signaling pathway was less activated during and after sepsis in the CXCR6^{+} T cell cluster than in the other T cell clusters, suggesting that IFNγ has little role in shaping the CXCR6^{+} tissue-resident compartment after sepsis (**Figure 4D).** We confirmed that sepsis increased the number of CXCR6^{+} tissue-resident cells in mice with deficiency in IFNγ receptors (**Figure 4E**), supporting the rationale to study receptor signaling pathways in addition to R-L correlations when investigating by single-cell RNA-sequencing the impact of the microenvironment on a specific cell type fate.

Among the predicted R-L interactions, we thoroughly studied the Cxcr6-Cxcl16 and Ccr2-Ccl2/Ccl6 pairs because their signaling pathways were selectively activated in the Cxcr6 T cell cluster (**Figure S6**), and their ligands were found in the macrophage cluster which is the cell cluster expressing the greatest number of potential ligands (**Figure 4C**). We observed that the percentages of Cxcl16 expressing cells and the Cxcl16 expression level were increased in the monocyte/macrophage clusters during and after sepsis (**Figure 4F**). We confirmed by flow cytometry the production of CXCL16 by resident alveolar macrophages during and after sepsis, while the number of CXCL16^{+} inflammatory macrophages rapidly decreased after sepsis (**Figure 4G**). To reveal the functional role of macrophages, we treated mice with a blocking anti-CXCL16 antibody from day 0 to day 7 of sepsis. The total number of tissue-resident CXCR6^{+} T cells was lower in sepsis-cured mice treated with anti-CXCL16 blocking antibody than in mice treated with isotype control (**Figure 4H).** Reproducing what was observed in genetically modified mice deficient for Cxcr6, the blocking of the CXCL16 mainly reduced the number of tissue-resident CXCR6^{+} γδ T cells but did not affect the number of resident CXCR6^{-} T cells (**Figure S7A-C**).

Regarding the Ccr2-Ccl6 pair, we observed that the percentages of Ccr2 expressing T cells increased during and after sepsis (**Figure 4I-J),** and the percentage of Ccl6 expressing cells in the monocyte/macrophage clusters decreased during sepsis but regained initial levels after the sepsis was cured (**Figure 4K**). The number of tissue-resident CXCR6$^+$ T cells was significantly lower after sepsis in genetically modified mice deficient in Ccr2 than in wild-type mice (**Figure 4L** and **Figures S7D-F**). In conclusion, we demonstrated that resident alveolar macrophages develop cytokine and chemokine networks during and after sepsis, which induce the local accumulation of tissue-resident T cells, mainly oriented toward γδ T cells, via CCR2 and CXCR6 receptors.

CCR2 increases CXCR6 expression, which extends T cells tissue residency after sepsis

To investigate the effects of CCR2 and CXCR6 on tissue-resident T cells, we tested whether they undergo proliferation in the lungs after sepsis. We found that the proliferation marker Ki67 was upregulated in CXCR6$^+$ but not in CXCR6$^-$ resident T cells (**Figure 5A**), supporting the hypothesis that lung CXCR6$^+$ T cells proliferated *in situ* after sepsis. This proliferation was associated with CXCR6 and not CCR2, as the expression of Ki67 in tissue-resident T cells was reduced in Cxcr6 deficient mice but not in Ccr2 deficient sepsis-cured mice (**Figures 5B-C**). Blocking CXCL16 also reduced the expression of the proliferation marker Ki67 in this population (**Figure 5D**), suggesting that CXCL16 produced by macrophages participates in the local proliferation of resident T cells during sepsis.

The rate of tissue egress needs to be finely tuned to enable the residency of proliferating T cells (*18*). We notably found that Ccr7 and S1pr1, two receptors associated with tissue egress (*24*, *25*), were not expressed in the CXCR6 cluster (**Figure S4**). We questioned if sepsis increases the ability of the lung tissue to induce T cell residency. To respond to this question, we transferred T cells collected from uninfected CD45.2$^+$ wild-type mice into the lungs of control or sepsis-cured CD45.1$^+$ recipients; then, we measured the number of transferred T cells in the recipient's lungs 36 hours later (*24*). We observed that the number of resident T cells from transferred cells retained in the lungs was increased in sepsis-cured recipient mice (**Figure 5E**). We repeated this experiment by transferring T cells from Cxcr6 or Ccr2 deficient donor mice into wild-type recipients and observed that sepsis did not increase the number of Cxcr6 deficient or Ccr2 deficient T cells retained in the lungs (**Figure 5F**), demonstrating the role of these receptors in the tissue residency of T cells after sepsis.

Taking advantage of the Cxcr6-deficient mice in which EGFP cDNA replaced the Cxcr6 coding region, we observed that the expression of the Cxcr6 reporter gene was increased when T cells were transferred into the lungs of sepsis-cured mice as compared to those transferred in uninfected recipients (**Figure 5G**). To explore the pathways of the lung microenvironment that increase the CXCR6 expression by T cells, we tested the correlation between the receptor expressions in the Cxcr6 T cell cluster and found that CXCR6 expression level was associated with *Ccr*2 and *Tgfβ-r2*, but not in other R-L pairs defined above (**Figure 5H**). We found that the level of expression of CXCR6 by resident T cells was decreased in septic-cured Ccr2-deficient mice (**Figure 5I**) and CCR2 deficient T cells transferred in the lungs of sepsis-cured wild-type mice (**Figure 5J)**, thus, demonstrating that CCR2 increases the CXCR6 expression by T cells. These results demonstrated that the post-septic lung niche makes T cells more suitable for residency via the CCR2-dependent upregulation of CXCR6 expression. Finally, we questioned if CXCR6 was only required to initiate T cells' residency or for its maintenance. To respond to this question, we transferred resident T cells collected in the lungs of sepsis-cured wild-type or Cxcr6 deficient CD45.2^{+} mice into the lungs of CD45.1^{+} uninfected recipients. We observed that the retention of Cxcr6 deficient transferred cells decreased (**Figure 5K**), demonstrating that CXCR6 was required to sustain the tissue residency of T cells.

Trained macrophages trigger the residency of T cells during secondary immune stimulation

While the number of CXCR6^{+} tissue-resident T cells picked on day seven after sepsis and then decreased afterward (**Figure 2F**), we have observed that these cells were higher during tumor growth in mice infected up to 56 days before (**Figure 2J)**. The accumulation of tissue-resident CXCR6^{+} T cells during immune re-stimulation was not specific to cancer since we observed a similar phenomenon during secondary pneumonia (**Figures 6A).** These observations suggested that the lung tissue does not continuously maintain a high number of CXCR6^{+} tissue-resident T after sepsis but can trigger these cells' residency in case of a second immune stimulation.

We questioned if the proportions of other immune cells were also altered during secondary immune stimulation or if the post-sepsis signature remains centered on CXCR6^{+} tissue-resident T. To respond to this question, we characterized by sc-RNA sequencing the immune cell composition of lung tissue on day 1, day 3, and day 7 of a secondary *E. coli* lung sepsis. We compared it to the time course of the immune response to primary *E. coli* sepsis. This high throughput analysis showed that the main difference was a higher proportion of the Cxcr6^{+} T cell cluster in mice cured

of secondary sepsis than in mice cured of primary sepsis (**Figure 6B and Figure S8A**). In secondary sepsis cured mice, these resident CXCR6$^+$ T cells were almost exclusively composed of IL17$^+$ Vγ6δ T cells (**Figure 6C-D and Figure S8B**), demonstrating an incremental specialization of the lung immune response for inducing the residency of tissue-resident Vγ6δ T cells.

We questioned if this observation was caused by some intrinsic capacities of the cells selected during the first sepsis or by mediators lingering in the local microenvironment. To respond to this question, we aimed to deplete a specific subpopulation of tissue-resident T cells and investigate if the microenvironment can reconstitute this cell pool during secondary sepsis. We thus depleted CXCR3$^+$ cells in sepsis-cured mice and measured the reconstitution of the CXCR3$^+$ CXCR6$^+$ resident γδ T pool during secondary sepsis (**Figure S8C)**. Despite the efficacy of the depletion, the number of resident CXCR3$^+$ CXCR6$^+$ resident γδ T cells was not different between sepsis-cured mice treated with the depleting antibody or isotype control (**Figure S8C**). This result demonstrated that the incremental accumulation of Vγ6δ T cells was independent of the T cells selected during the first sepsis and suggested that the local microenvironment mediators could restore the tissue-resident T cell number from the reduced cell pooled.

We thus investigated the immune mediators lingering in the lungs after sepsis, which increase the residency of T cells during a secondary immune challenge. We repeated the approach to create the R-L interactions atlas (see **Figure 4**) to predict the main pathways involved in the CXCR6$^+$ T cells residency during secondary sepsis. Compared to the R-L interactions map defined during the first sepsis, Cxcr6-Cxcl16 and Ccr2-Ccl2/Ccl6/Ccl7 couples were still found in mice cured of second sepsis, and macrophages still appeared as the primary source of potential ligands (**Figure 6E and Figure S8D**). Supporting the role of Ccr2-Ccl6 interactions, we found that the proportions of cells expressing Ccl6 in the monocyte/macrophages cluster and Ccr2 in the T cells compartment increased during secondary sepsis (**Figure 6F**). Regarding the Cxcr6-Cxcl16 couple, the proportion of Ccl6 expressing monocytes/macrophages and the Cxcr6 expression in the T cells compartment increased during the second sepsis (**Figure 6G**).

This series of analyses suggested that macrophages' capacity to induce the residency of CXCR6+ T cells during an immune challenge is increased in sepsis-cured animals. We hypothesized that this could be associated with the concept of trained innate immunity, recently defined as enhanced responsiveness of innate immune cells to subsequent stimulation after a first activation (*11*).

Trained immunity is characterized by epigenetic regulation of macrophages (*26*), and we have previously reported profound alterations of epigenetic regulation of resident alveolar macrophages in sepsis-cured mice (*13*). Re-analysing this Histone H3 Lysine 27 acetylation (H3K27ac) ChIP-seq data set, a chromatin mark associated with activation and trained immunity (*27*), we identified in resident alveolar macrophages harvested from sepsis-cured mice that H3K27ac peaks were increased in the Cxcl16 genomic region (**Figure 6H**) as well as in the genomic regions of chemokines and cytokines from the formerly developed L-R atlas (IL-1a, IL-1b and Inhba which is a member of the TGFβ family, **Figure S9A**), or known to be involved in T cell maintenance (IL-7, IL-15, Ccl3, Ccl9) (**Figure S9B**). We confirmed by flow cytometry that the proportion of $CXCL16^+$ resident alveolar macrophages was increased during secondary sepsis (**Figure 6I**). The production of CXCL16 by inflammatory macrophages was not increased during secondary pneumonia, arguing against a role of these cells in the immune lung specialization observed after sepsis (**Figure 6I**).

Finally, we aimed to therapeutically reproduce the accumulation of tissue-resident $CXCR6^+$ γδ T cells by injecting laminarin, a purified fraction of β-(1-3)-glucans known to induce trained immunity. Mice treated or not with laminarin were challenged by *E. coli* sepsis or LLC 7 days later. We observed that the number of resident CXCR6+ γδ T cells was increased after sepsis (**Figure 6J**) or during LLC development in mice pre-treated with laminarin (**Figure 6K**). Interestingly, reproducing what was observed after sepsis, the development of lung metastasis was decreased in mice pre-treated with laminarin (**Figure 6L**). This series of experiments demonstrates that trained macrophages have a sustained ability to increase tissue residency of T cells, specialized for γδ T cells, via epigenetic regulation of a chemokine and cytokine gene network and that it is possible to therapeutically reproduce this phenomenon by injecting β-(1-3)-glucans.

Extrapolation of the immune reprogramming defined in sepsis-cured mice in human lung tumor immunity

Given the proposed therapeutic potential of inducing residency of T cells to prevent and treat cancer, we aimed to confirm the association between $CXCR6^+$ tissue-resident T cells and cancer evolution in humans. CXCR6 can be expressed by T cells or cancer cells (*28*), and we thus first questioned if T cells are the main source of CXCR6. To answer this question, we performed immune histology analyses of the samples collected in humans surgically operated for lung

carcinoma and found co-localization of CD3 and CXCR6 (**Figure 7A**). We also examined RNA-seq datasets from publicly available databases of human tissue-resident T cells sorted from lung tumors (Gene Expression Omnibus SE111898 for lungs (*29*)) or the dermis (dataset GSE83637 (*30*)). We observed significant correlations between the CXCR6 expression level and gene signature of tissue-resident T cells in tumors, lung tissue, and dermis (**Figure 7B**), supporting the expression of CXCR6 by tissue-resident T cells in human tissues, including lung cancer.

We then questioned if the CXCR6 tissue-resident T cell population described in our mice model could be extrapolated to T cells infiltrating human lung tumors. To respond to this question, we defined a gene signature of tissue-resident T cells infiltrating human lung tumors from a publicly available data set (European Genome-Phenome Archive EGAS00001004707)(*31*). We found that the projection of this signature overlapped with the CXCR6 T cell cluster in the UMAP representation of single-cell RNA-seq of lung tissue from septic-cured mice (**Figure 7C**). We observed a similar result when projecting the gene signature of human dermis tissue-resident T cells on the mice dataset (**Figure S10A**). Considering the risk of bias with the projection of human signature on a mice dataset, we tested the expression level of the tissue-resident T cells gene signature defined in sepsis-cured mice (**Figure S10B)** in a human dataset. We found that the gene signature of tissue-resident T cells developed in sepsis-cured mice was enriched in tissue-resident memory T cells infiltrating human lung cancer compared to nonresident T cells (**Figure 7D**). All these results supported the extrapolation in tissue-resident T cells infiltrating human tumors of the gene signature of $CXCR6^+$ T cells enriched in septic-cured mice.

Then, we investigated the correlation between the lung tumor tissue-resident memory T cell (TRM) signature expression level with markers of tumor-associated macrophages (CD64, CD14, and CD68), Cxcl16, and potential CCR2 ligands (Ccl2 and Ccl7) in the human LUAD cancer TCGA database (**Figure 7E**). Cxcl16 expression was homogeneously highly expressed in patients and thus did not correlate with lung tumor tissue-resident T cell signature. However, the lung tumor TRM signature was associated with the tested macrophage markers and CCR2 ligands expression levels (**Figure 7E**). Macrophage markers and CCR2 ligand expression levels were also correlated. These correlations supported the role of the chemokine network released by macrophages in the accumulation of $CXCR6^+$ tissue-resident T cells in human lung tumors.

Ccr2 Cxcr6 co-expression level predicts survival in human cancer patients

Further supporting the extrapolation in humans of the role of CCR2 and CXCR6 expressions on tissue-resident T cells, we reported that Ccr2 correlated highly with Cxcr6 expression levels in LUAD RNA-seq dataset from the TCGA database (**Figure 7F**). Finally, we also compared the survival of humans with lung adenocarcinoma according to the level of expression of Cxcr6 and Ccr2 and found that patients with the highest Cxcr6_Ccr2 co-expression levels had a greater survival probability than the bottom third (**Figures 7F**). To assess the general relevance of CCR2 CXCR6 T cells for human cancer, we extended this analysis to several TCGA tumor types selecting those whose risks were decreased in the French cohort of sepsis survivors, such as cervical squamous cell cancer (pharynx), skin cutaneous melanoma and breast cancer. Hence, Ccr2 highly correlated with Cxcr6 expressions in these cancers, and $Cxcr6^{high}$ $Ccr2^{high}$ co-expression was associated with increased survival (**Figure 7G-I**).

INTERPRETATION

Sepsis is an overwhelming systemic inflammation induced by infection. This condition, associated with high mortality risk, demonstrates that developing an immune response mounted to eradicate pathogens can negatively impact the host's fitness. While innate immunity is central in the cytokine storm observed during sepsis, the training of mononuclear phagocytes, which alters their responsiveness to subsequent triggers, can be an essential mechanism for an individual to optimize the benefit-risk balance between immunopathology and tolerance throughout an individual's life. The immune reprogramming described after sepsis has been associated with susceptibility and resistance to secondary infections, depending on the agent causing the primary immune stimulation and the delay between the immune priming and the recall. With little information on the impact of sepsis-induced trained immunity on the risk of cancer available at the beginning of the project, we aimed to avoid implementing a hypothesis-driven approach during the mechanistic investigation in the mice model. We thus first gained access to and analyzed medical records from the national administrative health claims data on hospitalization to find that sepsis cure was associated with reduced cancer in humans. Then, bridging the gap between this observation made at a population level and experimental evidence, we observed that sepsis curation was associated with tissue enrichment of resident T cells, mainly $IL17^{+}$ $ROR\gamma t^{+}$ $V\gamma 6\delta$ T cells, and decreased risk of cancer development for years in humans and months in mice. The anti-tumor effects of sepsis were suppressed in CXCR6 deficient animals, in which tissue-resident T cells did not accumulate after

sepsis. Our data support a model in which resident alveolar macrophages are locally epigenetically trained at the time of sepsis, then develop cytokine and chemokine networks that induce tissue residency of proliferating T cells at the time of secondary cancer development. Laminarin, a purified fraction of β-(1-3)-glucan, was able to reproduce this protection and represent a novel approach to cancer immunotherapy by modulating tissue-resident cell anti-tumor activity.

While the inheritance of trained immunity and infection resistance has been demonstrated in mammals (*32*), bone marrow is proposed to be the primary site of training of the monocytic lineage (monocytes/macrophages) after sepsis (*14*). After respiratory sepsis, the training of resident alveolar macrophages lasts for months and is responsible for an early period of immunosuppression characterized by low phagocytic capacity (*13*), followed by a late period of resistance to bacterial infection through enhanced neutrophilia (*33*). Although a fraction of resident alveolar macrophages derives from the monocytes recruited in the lungs throughout life (*34*), the renewal of these cells develops mainly locally with a minimal contribution from bone-marrow precursors (*34*, *35*). The contribution of bone marrow progenitors thus appears facultative to induce the training of differentiated residential macrophages. Supporting this hypothesis, the identity and functions of resident macrophages continuously adapt to the modifications of their microenvironment (*36*), as demonstrated by the transformation of peritoneal macrophages into alveolar macrophages after adoptive transfer into lung tissue (*37*), or the loss of post-septic epigenetic regulation after transfer into uninfected recipient (*13*). We propose that the spatiotemporal adaptation of macrophages to their environment is an *in vivo* mechanism for inducing trained innate immunity in the periphery independently of bone-marrow progenitors. Here, we bring novelty by demonstrating that after sepsis, resident macrophages develop a chemokine and cytokine network that induces the residency of T cells, thus linking the concept of trained innate immunity with the control of tissue-resident T cell populations. Since regulatory T cells and CD8 T cells induce and maintain the training of mononuclear phagocytes via the production of TGFβ (*15*) and IFN-γ , respectively (*33*), the development of trained immunity in peripheral tissue thus appears as a mutual enrichment and refinement of the cross-regulations of resident innate and adaptative cells.

We found that sepsis-curation reduced tumor growth by accumulating tissue-resident $CXCR6^+$ T cells. This mechanism, which was demonstrated by the tumoral growth observed in Cxcr6-deficient sepsis-cured mice, which lack tissue-resident T cells, fits with the knowledge that tissue-resident T cells are important actors in the surveillance and control of subclinical cancer (*19*). The

tissue-resident T cells are heterogeneous, and we found that the main tissue-resident T cells accumulating after sepsis were IL17$^+$ RORγt Vγ6δ T cells. Given the capacity of γδ T cells to recognize malignant cells, infiltrate tumors, and cytotoxic activity, γδ T-cell therapies are being tested in humans with cancer (*38*). In mice treated with β-glucan, increased neutrophil recruitment induced by trained granulopoiesis promoted anti-tumoral activities(*39*), demonstrating that an inflammatory response boost can be protective in this setting. However, Vγ6$^+$Vδ1$^+$ T cells promote tumor cell proliferation in case of chronic bacterial colonization, notably by increasing the recruitment of neutrophils and protracting the inflammatory lung response (*40*). This discrepancy can be explained by the balance between pro-and anti-tumoral effects of IL-17$^+$ γδ T cells, which are tuned by the host-microbiome interactions and the duration of the inflammatory response. To unify these observations, we showed that sepsis-induced trained immunity is not associated with a permanent and chronic accumulation of tissue-resident IL17$^+$ γδ T cells but enables the tissues to induce the residency of newly proliferating γδ T at the time of a subsequent immune stimulation. We propose that this trigger-effect enhances the tissue response to potential cancer development without exposing the organs to the adverse effects of chronic inflammation.

While T cell-targeted approaches are highly efficient against several cancer types, increasing the capacity of macrophages to induce T cell residency can reduce treatment failure rates or prevent cancer in high-risk patients. We observed a CCR2-dependent increase in the membrane expression of CXCR6, while CXCR6 subsequently sustains the tissue residency of γδ T cells. To propose this original chemokine and cytokine network, we have exploited the high throughput characterization of the immune landscape by sc-RNA-sequencing of lung tissue. This approach has already been used to understand basophils' training of alveolar macrophages at birth (*22*). Here, we repeated this approach to develop an atlas of predicted R-L interactions. Given the long list of potential L-R couples generated here, it is vital to hierarchize the most important ones. Here, we completed the observation of L-R correlation with the analyses of the gene ontology in tissue-resident T cells to confirm the activation of relevant pathways. We notably observed that while IFNγR and IFNγ were expressed, the interferon-stimulated gene response elements were not increased in CXCR6 T cells after sepsis, arguing against a role of type II interferon in T cell residency after sepsis. We validated this approach by confirming that the number of resident CXCR6 T cells was not altered in sepsis-cure mice deficient in IFNγR.

We show that trained innate immunity regulates several critical immune functions, including tissue residency of T cells. Reinforcing this physiological process in patients at high risk of developing cancer or recurrency could increase the efficacy of T-cell-targeted therapies. B-glucans are a broad family of β-D-glucose polysaccharides naturally found in fungi, bacteria, or vegetal cell walls. This capacity of this family to train innate immunity is well recognized (*41*, *42*), yet the broad heterogeneity of the polysaccharide compositions used in previous studies has precluded the development of purified β-glucan as an approved drug for immunomodulation in humans. The investigation of the minimal chains and motifs required to maintain the immunostimulant activities of β-glucans (*43*), should help pave the way to an approved drug for cancer treatment. Here, we have been able to mimic the effects of sepsis by injecting a low-molecular-weight fraction of laminarin from the brown seaweed *Laminaria digitate.* This β-(1,3)-glucan is composed of ~25 linear glucosyl units (average molecular weight of 4 kDa), with one branched entity randomly substituted at a 6-position (*44*). Further characterizing this fraction of laminarin, we have identified that non-reducing mannitol residues, which represent up to 30% of the polysaccharide, had no impact on the immunostimulant properties (*45–47*), while a short sequence of six glucosyl units is necessary to interact with Dectin-1 efficiently, the primary receptor for the β-(1,3)-glucans (*43*).

Our results can be summarized in four main findings: (i) sepsis reduces long-term tumor growth by increasing the number of tissue-resident CXCR6^{+} T cells, IL17^{+} RORγt^{+} Vγ6δ T cells being the most likely subset mediating this effect; (ii) trained macrophages develop a cytokine and chemokine network that increases tissue residency of T cells during secondary immune trigger (**Graphical abstract**); (iii) induction of trained immunity by laminarin may represent a therapeutic strategy to increase T cell residency and reduce the risk of tumor recurrence in patients; (iv) Ccr2-Cxcr6 signature in human tumors can help to predict survival. Our study indicates a new mechanism of the long-term immune effects of sepsis, linking trained innate immunity to the regulation of tissue-residency of T cells and cancer immune surveillance.

References and Notes

1. G. 2016 L. R. I. Collaborators, Estimates of the global, regional, and national morbidity, mortality, and aetiologies of lower respiratory infections in 195 countries, 1990–2016: a systematic analysis for the Global Burden of Disease Study 2016. *Lancet Infect Dis*. 18, 1191–1210 (2018).

2. I. Lakbar, M. Munoz, V. Pauly, V. Orleans, C. Fabre, G. Fond, J.-L. Vincent, L. Boyer, M. Leone, Septic shock: incidence, mortality and hospital readmission rates in French intensive care units from 2014 to 2018. *Anaesth Crit Care Pa*. 41, 101082 (2022).

3. M. Singer, C. S. Deutschman, C. W. Seymour, M. Shankar-Hari, D. Annane, M. Bauer, R. Bellomo, G. R. Bernard, J.-D. Chiche, C. M. Coopersmith, R. S. Hotchkiss, M. M. Levy, J. C. Marshall, G. S. Martin, S. M. Opal, G. D. Rubenfeld, T. van der Poll, J.-L. Vincent, D. C. Angus, The Third International Consensus Definitions for Sepsis and Septic Shock (Sepsis-3). *Jama*. 315, 801–810 (2016).

4. K.-M. Kaukonen, M. Bailey, D. Pilcher, D. J. Cooper, R. Bellomo, Systemic Inflammatory Response Syndrome Criteria in Defining Severe Sepsis. *New Engl J Medicine*. 372, 1629–1638 (2015).

5. D. C. Fajgenbaum, C. H. June, Cytokine Storm. *New Engl J Med*. 383, 2255–2273 (2020).

6. M. Shankar-Hari, M. Ambler, V. Mahalingasivam, A. Jones, K. Rowan, G. D. Rubenfeld, Evidence for a causal link between sepsis and long-term mortality: a systematic review of epidemiologic studies. *Crit Care*. 20, 101 (2016).

7. P. N. Sipilä, N. Heikkilä, J. V. Lindbohm, C. Hakulinen, J. Vahtera, M. Elovainio, S. Suominen, A. Väänänen, A. Koskinen, S. T. Nyberg, J. Pentti, T. E. Strandberg, M. Kivimäki, Hospital-treated infectious diseases and the risk of dementia: a large, multicohort, observational study with a replication cohort. *Lancet Infect Dis*. 21, 1557–1567 (2021).

8. V. F. Corrales-Medina, K. N. Alvarez, L. A. Weissfeld, D. C. Angus, J. A. Chirinos, C.-C. H. Chang, A. Newman, L. Loehr, A. R. Folsom, M. S. Elkind, M. F. Lyles, R. A. Kronmal, S. Yende, Association Between Hospitalization for Pneumonia and Subsequent Risk of Cardiovascular Disease. *Jama*. 313, 264–274 (2015).

9. M. Bouras, K. Asehnoune, A. Roquilly, Contribution of Dendritic Cell Responses to Sepsis-Induced Immunosuppression and to Susceptibility to Secondary Pneumonia. *Front Immunol*. 9, 2590 (2018).

10. I. Rubio, M. F. Osuchowski, M. Shankar-Hari, T. Skirecki, M. S. Winkler, G. Lachmann, P. L. Rosée, G. Monneret, F. Venet, M. Bauer, F. M. Brunkhorst, M. Kox, J.-M. Cavaillon, F. Uhle, M. A. Weigand, S. B. Flohé, W. J. Wiersinga, M. Martin-Fernandez, R. Almansa, I. Martin-Loeches, A. Torres, E. J. Giamarellos-Bourboulis, M. Girardis, A. Cossarizza, M. G. Netea, T. van der Poll, A. Scherag, C. Meisel, J. C. Schefold, J. F. Bermejo-Martín, Current gaps in sepsis immunology: new opportunities for translational research. *Lancet Infect Dis*. 19, e422–e436 (2019).

11. M. G. Netea, J. Domínguez-Andrés, L. B. Barreiro, T. Chavakis, M. Divangahi, E. Fuchs, L. A. B. Joosten, J. W. M. van der Meer, M. M. Mhlanga, W. J. M. Mulder, N. P. Riksen, A. Schlitzer, J. L. Schultze, C. S. Benn, J. C. Sun, R. J. Xavier, E. Latz, Defining trained immunity and its role in health and disease. *Nat Rev Immunol*. 20, 375–388 (2020).

12. L. A. van Vught, P. M. C. K. Klouwenberg, C. Spitoni, B. P. Scicluna, M. A. Wiewel, J. Horn, M. J. Schultz, P. Nürnberg, M. J. M. Bonten, O. L. Cremer, T. van der Poll, Incidence, Risk Factors, and Attributable Mortality of Secondary Infections in the Intensive Care Unit After Admission for Sepsis. *Jama*. 315, 1469 (2016).

13. A. Roquilly, C. Jacqueline, M. Davieau, A. Mollé, A. Sadek, C. Fourgeux, P. Rooze, A. Broquet, B. Misme-Aucouturier, T. Chaumette, M. Vourc'h, R. Cinotti, N. Marec, V. Gauttier, H. E. G. McWilliam, F. Altare, J. Poschmann, J. A. Villadangos, K. Asehnoune, Alveolar macrophages are epigenetically altered after inflammation, leading to long-term lung immunoparalysis. *Nat Immunol*. 21, 636–648 (2020).

14. B. Cirovic, L. C. J. de Bree, L. Groh, B. A. Blok, J. Chan, W. J. F. M. van der Velden, M. E. J. Bremmers, R. van Crevel, K. Händler, S. Picelli, J. Schulte-Schrepping, K. Klee, M. Oosting, V. A. C. M. Koeken, J. van Ingen, Y. Li, C. S. Benn, J. L. Schultze, L. A. B. Joosten, N. Curtis, M. G. Netea, A. Schlitzer, BCG Vaccination in Humans Elicits Trained Immunity via the Hematopoietic Progenitor Compartment. *Cell Host Microbe*. 28, 322-334.e5 (2020).

15. A. Roquilly, H. E. G. McWilliam, C. Jacqueline, Z. Tian, R. Cinotti, M. Rimbert, L. Wakim, I. Caminschi, M. H. Lahoud, G. T. Belz, A. Kallies, J. D. Mintern, K. Asehnoune, J. A. Villadangos, Local Modulation of Antigen-Presenting Cell Development after Resolution of Pneumonia Induces Long-Term Susceptibility to Secondary Infections. *Immunity*. 47, 135-147.e5 (2017).

16. P. M. Ridker, J. G. MacFadyen, T. Thuren, B. M. Everett, P. Libby, R. J. Glynn, P. Ridker, A. Lorenzatti, H. Krum, J. Varigos, P. Siostrzonek, P. Sinnaeve, F. Fonseca, J. Nicolau, N. Gotcheva, J. Genest, H. Yong, M. Urina-Triana, D. Milicic, R. Cifkova, R. Vettus, W. Koenig, S. D. Anker, A. J. Manolis, F. Wyss, T. Forster, A. Sigurdsson, P. Pais, A. Fucili, H. Ogawa, H. Shimokawa, I. Veze, B. Petrauskiene, L. Salvador, J. Kastelein, J. H. Cornel, T. O. Klemsdal, F. Medina, A. Budaj, L. Vida-Simiti, Z. Kobalava, P. Otasevic, D. Pella, M. Lainscak, K.-B. Seung, P. Commerford, M. Dellborg, M. Donath, J.-J. Hwang, H. Kultursay, M. Flather, C. Ballantyne, S. Bilazarian, W. Chang, C. East, B. Everett, L. Forgosh, R. Glynn, B. Harris, P. Libby, M. Ligueros, T. Thuren, E. Bohula, B. Charmarthi, S. Cheng, S. Chou, J. Danik, G. McMahon, B. Maron, M. Ning, B. Olenchock, R. Pande, T. Perlstein, A. Pradhan, N. Rost, A. Singhal, V. Taqueti, N. Wei, H. Burris, A. Cioffi, A. M. Dalseg, N. Ghosh, J. Gralow, T. Mayer, H. Rugo, V. Fowler, A. P. Limaye, S. Cosgrove, D. Levine, R. Lopes, J. Scott, T. Thuren, M. Ligueros, R. Hilkert, G. Tamesby, C. Mickel, B. Manning, J. Woelcke, M. Tan, S. Manfreda, T. Ponce, J. Kam, R. Saini, K. Banker, T. Salko, P. Nandy, R. Tawfik, G. O'Neil, S. Manne, P. Jirvankar, S. Lal, D. Nema, J. Jose, R. Collins, K. Bailey, R. Blumenthal, H. Colhoun, B. Gersh, R. J. Glynn, Effect of interleukin-1β inhibition with canakinumab on incident lung cancer in patients with atherosclerosis: exploratory results from a randomised, double-blind, placebo-controlled trial. *Lancet*. 390, 1833–1842 (2017).

17. A. N. Wein, S. R. McMaster, S. Takamura, P. R. Dunbar, E. K. Cartwright, S. L. Hayward, D. T. McManus, T. Shimaoka, S. Ueha, T. Tsukui, T. Masumoto, M. Kurachi, K. Matsushima, J. E. Kohlmeier, CXCR6 regulates localization of tissue-resident memory CD8 T cells to the airways. *J Exp Medicine*. 216, 2748–2762 (2019).

18. S. N. Mueller, L. K. Mackay, Tissue-resident memory T cells: local specialists in immune defence. *Nat Rev Immunol*. 16, 79–89 (2016).

19. S. L. Park, A. Buzzai, J. Rautela, J. L. Hor, K. Hochheiser, M. Effern, N. McBain, T. Wagner, J. Edwards, R. McConville, J. S. Wilmott, R. A. Scolyer, T. Tüting, U. Palendira, D. Gyorki, S. N. Mueller, N. D. Huntington, S. Bedoui, M. Hölzel, L. K. Mackay, J. Waithman, T. Gebhardt, Tissue-resident memory CD8+ T cells promote melanoma–immune equilibrium in skin. *Nature*. 565, 366–371 (2019).

20. N. S. Wilson, G. M. N. Behrens, R. J. Lundie, C. M. Smith, J. Waithman, L. Young, S. P. Forehan, A. Mount, R. J. Steptoe, K. D. Shortman, T. F. de Koning-Ward, G. T. Belz, F. R. Carbone, B. S. Crabb, W. R. Heath, J. A. Villadangos, Systemic activation of dendritic cells by Toll-like receptor ligands or malaria infection impairs cross-presentation and antiviral immunity. *Nat Immunol*. 7, 165–172 (2006).

21. X. Zhou, R. A. Franklin, M. Adler, J. B. Jacox, W. Bailis, J. A. Shyer, R. A. Flavell, A. Mayo, U. Alon, R. Medzhitov, Circuit Design Features of a Stable Two-Cell System. *Cell*. 172, 744-757.e17 (2018).

22. M. Cohen, A. Giladi, A.-D. Gorki, D. G. Solodkin, M. Zada, A. Hladik, A. Miklosi, T.-M. Salame, K. B. Halpern, E. David, S. Itzkovitz, T. Harkany, S. Knapp, I. Amit, Lung Single-Cell Signaling Interaction Map Reveals Basophil Role in Macrophage Imprinting. *Cell*. 175, 1031-1044.e18 (2018).

23. S. N. Christo, M. Evrard, S. L. Park, L. C. Gandolfo, T. N. Burn, R. Fonseca, D. M. Newman, Y. O. Alexandre, N. Collins, N. M. Zamudio, F. Souza-Fonseca-Guimaraes, D. G. Pellicci, D. Chisanga, W. Shi, L. Bartholin, G. T. Belz, N. D. Huntington, A. Lucas, M. Lucas, S. N. Mueller, W. R. Heath, F. Ginhoux, T. P. Speed, F. R. Carbone, A. Kallies, L. K. Mackay, Discrete tissue microenvironments instruct diversity in resident memory T cell function and plasticity. *Nat Immunol*. 22, 1140–1151 (2021).

24. S. K. Bromley, S. Y. Thomas, A. D. Luster, Chemokine receptor CCR7 guides T cell exit from peripheral tissues and entry into afferent lymphatics. *Nat Immunol*. 6, 895–901 (2005).

25. C. N. Skon, J.-Y. Lee, K. G. Anderson, D. Masopust, K. A. Hogquist, S. C. Jameson, Transcriptional downregulation of S1pr1 is required for the establishment of resident memory CD8+ T cells. *Nat Immunol*. 14, 1285–1293 (2013).

26. S. Saeed, J. Quintin, H. H. D. Kerstens, N. A. Rao, A. Aghajanirefah, F. Matarese, S.-C. Cheng, J. Ratter, K. Berentsen, M. A. van der Ent, N. Sharifi, E. M. Janssen-Megens, M. T. Huurne, A. Mandoli, T. van Schaik, A. Ng, F. Burden, K. Downes, M. Frontini, V. Kumar, E. J. Giamarellos-Bourboulis, W. H. Ouwehand, J. W. M. van der Meer, L. A. B. Joosten, C.

Wijmenga, J. H. A. Martens, R. J. Xavier, C. Logie, M. G. Netea, H. G. Stunnenberg, Epigenetic programming of monocyte-to-macrophage differentiation and trained innate immunity. *Science*. 345, 1251086 (2014).

27. A. R. DiNardo, M. G. Netea, D. M. Musher, Postinfectious Epigenetic Immune Modifications — A Double-Edged Sword. *New Engl J Med*. 384, 261–270 (2021).

28. J. T. LEE, S. D. LEE, J. Z. LEE, M. K. CHUNG, H. K. HA, Expression analysis and clinical significance of CXCL16/CXCR6 in patients with bladder cancer. *Oncol Lett*. 5, 229–235 (2012).

29. J. Clarke, B. Panwar, A. Madrigal, D. Singh, R. Gujar, O. Wood, S. J. Chee, S. Eschweiler, E. V. King, A. S. Awad, C. J. Hanley, K. J. McCann, S. Bhattacharyya, E. Woo, A. Alzetani, G. Seumois, G. J. Thomas, A.-P. Ganesan, P. S. Friedmann, T. Sanchez-Elsner, F. Ay, C. H. Ottensmeier, P. Vijayanand, Single-cell transcriptomic analysis of tissue-resident memory T cells in human lung cancer. *J Exp Medicine*. 216, 2128–2149 (2019).

30. S. Cheuk, H. Schlums, I. G. Sérézal, E. Martini, S. C. Chiang, N. Marquardt, A. Gibbs, E. Detlofsson, A. Introini, M. Forkel, C. Höög, A. Tjernlund, J. Michaëlsson, L. Folkersen, J. Mjösberg, L. Blomqvist, M. Ehrström, M. Ståhle, Y. T. Bryceson, L. Eidsmo, CD49a Expression Defines Tissue-Resident CD8+ T Cells Poised for Cytotoxic Function in Human Skin. *Immunity*. 46, 287–300 (2017).

31. S. Corgnac, I. Malenica, L. Mezquita, E. Auclin, E. Voilin, J. Kacher, H. Halse, L. Grynszpan, N. Signolle, T. Dayris, M. Leclerc, N. Droin, V. de Montpréville, O. Mercier, P. Validire, J.-Y. Scoazec, C. Massard, S. Chouaib, D. Planchard, J. Adam, B. Besse, F. Mami-Chouaib, CD103+CD8+ TRM Cells Accumulate in Tumors of Anti-PD-1-Responder Lung Cancer Patients and Are Tumor-Reactive Lymphocytes Enriched with Tc17. *Cell Reports Medicine*. 1, 100127 (2020).

32. N. Katzmarski, J. Domínguez-Andrés, B. Cirovic, G. Renieris, E. Ciarlo, D. L. Roy, K. Lepikhov, K. Kattler, G. Gasparoni, K. Händler, H. Theis, M. Beyer, J. W. M. van der Meer, L. A. B. Joosten, J. Walter, J. L. Schultze, T. Roger, E. J. Giamarellos-Bourboulis, A. Schlitzer, M. G. Netea, Transmission of trained immunity and heterologous resistance to infections across generations. *Nat Immunol*. 22, 1382–1390 (2021).

33. Y. Yao, M. Jeyanathan, S. Haddadi, N. G. Barra, M. Vaseghi-Shanjani, D. Damjanovic, R. Lai, S. Afkhami, Y. Chen, A. Dvorkin-Gheva, C. S. Robbins, J. D. Schertzer, Z. Xing, Induction of Autonomous Memory Alveolar Macrophages Requires T Cell Help and Is Critical to Trained Immunity. *Cell*. 175, 1634-1650.e17 (2018).

34. S. Yona, K.-W. Kim, Y. Wolf, A. Mildner, D. Varol, M. Breker, D. Strauss-Ayali, S. Viukov, M. Guilliams, A. Misharin, D. A. Hume, H. Perlman, B. Malissen, E. Zelzer, S. Jung, Fate Mapping Reveals Origins and Dynamics of Monocytes and Tissue Macrophages under Homeostasis. *Immunity*. 38, 79–91 (2013).

35. M. Guilliams, G. R. Thierry, J. Bonnardel, M. Bajenoff, Establishment and Maintenance of the Macrophage Niche. *Immunity*. 52, 434–451 (2020).

36. A. Roquilly, J. D. Mintern, J. A. Villadangos, Spatiotemporal Adaptations of Macrophage and Dendritic Cell Development and Function. *Annu Rev Immunol*. 40 (2022), doi:10.1146/annurev-immunol-101320-031931.

37. Y. Lavin, D. Winter, R. Blecher-Gonen, E. David, H. Keren-Shaul, M. Merad, S. Jung, I. Amit, Tissue-Resident Macrophage Enhancer Landscapes Are Shaped by the Local Microenvironment. *Cell*. 159, 1312–1326 (2014).

38. T. Hoeres, M. Smetak, D. Pretscher, M. Wilhelm, Improving the Efficiency of Vγ9Vδ2 T-Cell Immunotherapy in Cancer. *Front Immunol*. 9, 800 (2018).

39. L. Kalafati, I. Kourtzelis, J. Schulte-Schrepping, X. Li, A. Hatzioannou, T. Grinenko, E. Hagag, A. Sinha, C. Has, S. Dietz, A. M. de J. Domingues, M. Nati, S. Sormendi, A. Neuwirth, A. Chatzigeorgiou, A. Ziogas, M. Lesche, A. Dahl, I. Henry, P. Subramanian, B. Wielockx, P. Murray, P. Mirtschink, K.-J. Chung, J. L. Schultze, M. G. Netea, G. Hajishengallis, P. Verginis, I. Mitroulis, T. Chavakis, Innate Immune Training of Granulopoiesis Promotes Anti-tumor Activity. *Cell*. 183, 771-785.e12 (2020).

40. C. Jin, G. K. Lagoudas, C. Zhao, S. Bullman, A. Bhutkar, B. Hu, S. Ameh, D. Sandel, X. S. Liang, S. Mazzilli, M. T. Whary, M. Meyerson, R. Germain, P. C. Blainey, J. G. Fox, T. Jacks, Commensal Microbiota Promote Lung Cancer Development via γδ T Cells. *Cell*. 176, 998-1013.e16 (2019).

41. B. Novakovic, E. Habibi, S.-Y. Wang, R. J. W. Arts, R. Davar, W. Megchelenbrink, B. Kim, T. Kuznetsova, M. Kox, J. Zwaag, F. Matarese, S. J. van Heeringen, E. M. Janssen-Megens, N. Sharifi, C. Wang, F. Keramati, V. Schoonenberg, P. Flicek, L. Clarke, P. Pickkers, S. Heath, I. Gut, M. G. Netea, J. H. A. Martens, C. Logie, H. G. Stunnenberg, β-Glucan Reverses the Epigenetic State of LPS-Induced Immunological Tolerance. *Cell*. 167, 1354-1368.e14 (2016).

42. M. Divangahi, P. Aaby, S. A. Khader, L. B. Barreiro, S. Bekkering, T. Chavakis, R. van Crevel, N. Curtis, A. R. DiNardo, J. Dominguez-Andres, R. Duivenwoorden, S. Fanucchi, Z. Fayad, E. Fuchs, M. Hamon, K. L. Jeffrey, N. Khan, L. A. B. Joosten, E. Kaufmann, E. Latz, G. Matarese, J. W. M. van der Meer, M. Mhlanga, S. J. C. F. M. Moorlag, W. J. M. Mulder, S. Naik, B. Novakovic, L. O'Neill, J. Ochando, K. Ozato, N. P. Riksen, R. Sauerwein, E. R. Sherwood, A. Schlitzer, J. L. Schultze, M. H. Sieweke, C. S. Benn, H. Stunnenberg, J. Sun, F. L. van de Veerdonk, S. Weis, D. L. Williams, R. Xavier, M. G. Netea, Trained immunity, tolerance, priming and differentiation: distinct immunological processes. *Nat Immunol*. 22, 2–6 (2021).

43. B. Sylla, L. Legentil, S. Saraswat-Ohri, A. Vashishta, R. Daniellou, H.-W. Wang, V. Vetvicka, V. Ferrières, Oligo-β-(1 → 3)-glucans: Impact of Thio-Bridges on Immunostimulating Activities and the Development of Cancer Stem Cells. *J Med Chem*. 57, 8280–8292 (2014).

44. F. Paris, S. Trouvelot, M. Jubien, G. Lecollinet, J.-M. Joubert, A. Chiltz, M.-C. Héloir, J. Negrel, M. Adrian, L. Legentil, X. Daire, V. Ferrières, Hydrophobized laminarans as new biocompatible anti-oomycete compounds for grapevine protection. *Carbohyd Polym*. 225, 115224 (2019).

45. K. Descroix, V. Větvička, I. Laurent, F. Jamois, J.-C. Yvin, V. Ferrières, New oligo-β-(1,3)-glucan derivatives as immunostimulating agents. *Bioorgan Med Chem*. 18, 348–357 (2010).

46. V. Vetvicka, S. Saraswat-Ohri, A. Vashishta, K. Descroix, F. Jamois, J.-C. Yvin, V. Ferrières, New 4-deoxy-(1→3)-β-d-glucan-based oligosaccharides and their immunostimulating potential. *Carbohyd Res*. 346, 2213–2221 (2011).

47. S. Saraswat-Ohri, A. Vashishta, V. Vetvicka, K. Descroix, F. Jamois, J.-C. Yvin, V. Ferrières, Biological Properties of (1 → 3)-β-d-Glucan-Based Synthetic Oligosaccharides. *J Med Food*. 14, 369–376 (2011).

Acknowledgments:

We thank Lucas Brusselle for helping with the preparation of single-cell libraries, Marine Papot for preparing the ligand-receptors analyses, and Emmanuelle Sechet for administrative support. We thank the Cytometry Facility "Cytocell," University of Nantes, and the Genomics and Bioinformatics Core Facility of Nantes (GenoBiRD, Biogenouest) for their technical support. We thank the Cytometry Facility Cytocell from Nantes for expert technical assistance. We acknowledge the IBISA MicroPICell facility (Biogenouest), member of the national infrastructure France-Bioimaging supported by the French National Research Agency (ANR-10-INBS-04). We thank the biological resource centre for biobanking (CHU Nantes, Hôtel Dieu, Tumorothèque, Nantes, F-44093, France»

Funding:

La Ligue Contre le Cancer (AB) and

"Association pour la Recherche sur le Cancer", ARC, grant SIGN'IT20181007792 (AB).

Agence National de la Recherche, grant ANR JCJC Progr-AM (AR)

ITMO Cancer of Aviesan, framework of the 2021-2030 (AR)

Author contributions:

Conceptualization: AB, JP, AR

Methodology: AB, VG, TG, LL, VF, CH, ES, SC, FMC, NM, JAV, PAG, KA, JP, AR

Investigation: AB, VG, TG, VLM, DS, MA, CJ, FPM, CP, CF, MC, TL, MG, TC

Visualization: AB, VG, TG, VLM, DS, MA, CJ, FPM, CP, CF, MC, TL, MG, TC

Funding acquisition: AB, AR

Project administration: AR

Supervision: CH, ES, SC, FMC, NM, JAV, PAG, KA, JP, AR

Writing – original draft: JP, AR

Writing – review & editing: AB, VG, TG, VLM, DS, MA, CJ, FPM, CP, CF, MC, TL, MG, TC, LL, VF, CH, ES, SC, FMC, NM, JAV, PAG, KA

Competing interests: Authors declare that they have no competing interests.

Data and materials availability: Correspondence and material requests should be addressed to Antoine Roquilly. Single-cell sequencing data supporting this study's findings have been deposited in ENA with the PRJEB52332 accession code (https://www.ebi.ac.uk/ena/browser/home). All data are available in the main text or the supplementary materials.

Supplementary Materials

Materials and Methods

Population. Every adult patient admitted to a mainland French hospital from January 1st, 2010, to December 31st, 2016, for trauma, pneumonia, or stroke was included in the initial sample. We ended inclusion in 2016 to ensure a minimum follow-up of 3 years for patients. A list of ICD-10 codes used to include patients is available in Appendix A. We were interested in whether or not the patient was admitted to an intensive care unit (SIRS yes/no) or whether or not the patient was infected while in the hospital (Sepsis/Aseptic). Infection may be the main reason for admission, or it may have been contracted during the stay. Patients with a history of cancer or autoimmune disease were excluded, as were patients who developed these conditions within one year of inclusion. Patients who died within 6 months of admission were also excluded. Some patients had multiple hospital stays during the study period. In order to retain only one stay per patient, we have first privileged stays with admission in the intensive care unit, if any, and then we retain the oldest stay.

Data. We collected data on age, sex, year, and month of hospitalization, admitting hospital, status concerning alcohol dependence, whether or not the patient suffers from obesity, and the time between admission and the first hospitalization with cancer as the primary diagnosis (main outcome) and cancer location. ICD-10 codes are also available in Appendix A for outcomes. Socio-economic data of patients' areas of residence were collected: percentage of single-parent families among households (average from 2013 to 2016, INSEE - *Institut National de la Statistique*

et des Études Économiques - National Institute of Statistics and Economic Studies), percentage of non-graduates people in the working population (average from 2009 to 2016, INSEE), percentage of workers in the working population (average from 2009 to 2016, INSEE) and percentage of unemployed persons in the working population (average from 2009 to 2016, INSEE). All these SNDS data were available from the ATIH data access platform. ATIH is a French public institution in charge of collecting, hosting, and analyzing data from health care institutions to ensure the technical management of the institutions' financing mechanisms. Through this institution, we had access to data collected within the PMSI (*Programme de Médicalisation des Systèmes d'Information* - Information systems medicalization program) over the last ten years from the acceptance of the study.

Handling of biases. To limit the effect of known or suspected confounding factors when comparing the occurrence of cancers outcomes between the groups defined by our main exposure factor, i.e., having stayed in an intensive care unit, we performed a 1:1 matching on age (± 5 years), sex, year of admission, admitting hospital (exact), alcohol dependence problem, obesity, percentage of single-parent families among households (± 5%), percentage of non-graduates people in the working population (± 5%), percentage of workers in the working population (± 5%) and percentage of unemployed persons in the working population (± 5%). This matching design allowed us to match a large percentage of the patients of interest while maintaining a geographical and socio-economic anchor between septic and infected patients. In this way, controls do not necessarily come from the same area of residence as the exposed patients, but from a similar area in terms of the 4 socio-economic variables mentioned above, and they were admitted to the same hospital. The matching process was assessed by looking at the differences in standardized means (SMD) of the characteristics between groups.

Statistical Analyses. Continuous variables are presented as mean plus standard deviation or as median plus interquartile range if non-normally distributed. Categorical variables are described as numbers and percentages. Missing values are systematically presented. Due to the large sample sizes, we did not use univariable comparison tests. To answer study objectives, we computed cumulative incidence curves and relative risks within groups by taking care to remove from the denominator at each time step the patients who died or declared the outcome at the previous time step or those for whom the follow-up did not go beyond. P-values for cumulative incidence curves comparison are obtained using ANCOVA, assuming that they can be interpreted as linear regression lines. Analyses were carried out using R software (version 4.0.2, available on ATIH

data access platform), mainly using the packages *dplyr* (https://CRAN.R-project.org/package=dplyr) and *data.table* (https://CRAN.R-project.org/package=data.table) for data manipulation, *tableone* for table creation (https://CRAN.R-project.org/package=tableone), ggplot2 for visualization, and Matching for propensity score pair-matching [49].

Mice and treatment. Mice used were C57BL/6J (B6), B6.SJL-PtprcaPep3b/BoyJ (Ly5.1), B6.129P2-Cxcr6tm1Litt/J (cxcr6$^{-/-}$), B6.129S4-Ccr2tm1lfc/J (ccr2$^{-/-}$), C57BL/6-Tg(TcraTcrb)1100Mjb/Crl (OT-I), B6.129S7-Ifngr1tm1Agt/J (IFNgR1$^{-/-}$). For technical reasons, mice were used for experiments without taking gender into account. Male and female mice were maintained in specific-pathogen-free conditions (group-housed) at the UTE-IRS2 Nantes Biotech Animal Facility (Nantes, France) following institutional guidelines and were used for experiments between 6 and 14 weeks of age. Experimental procedures were approved by the Animal Ethics Committee of the Pays de la Loire (APAFIS no. 27742-2020101514264674 v4). Laminarin was administrated i.v. (1mg/mouse), kindly provided by Drs. Legentil and Ferrieres.

Induction of pneumonia. *Escherichia coli* (E. coli. DH5α strain) or *Staphylococcus aureus* (), grown for 18 h in Luria broth medium at 37 °C, were washed twice (1,000*g*, 10 min, 37 °C), diluted in sterile isotonic saline and calibrated by nephelometry. Bacteria (75 µl, OD_{600} = 0.6–0.7) were injected intratracheally in anesthetized mice to induce non-lethal acute pneumonia. Pneumonia status is defined as ongoing pneumonia (days 1 to 3) and sepsis-cured (Day 7) [13,15]. For rechallenge experiments, 7 days or 28 days of sepsis-cured animals were subjected to secondary *E. coli* pneumonia for 7 days.

CpG injection. Mice were injected intravenously in the tail vein with 20 nmol of synthetic CpG1668 (20mer) 5'-T*C*C*A*T*G*A*C*G*T*T*C*C*T*G*A*T*G*C*T (Bioneer) dissolved in 200 µl of PBS.

Tissues dissociation. Lungs were excised after perfusing with PBS and minced with scissors into pieces, and digested 45′ at 37 °C in 5mL RPMI containing 2% fetal calf serum (FCS), 0,7% type-3 collagenase (Worthington, Freehold, USA), and 0.1% DNase I (Sigma Aldrich). Two cm-long pieces of the small intestine, after removal of any mesenteric lymph node, were minced with scissors into pieces and were digested for 1 hour at room temperature in 2 ml RPMI containing 2% FCS, 0.7% type-3 collagenase, 0.1% DNase I, and 0.05% Liberase TL (Roche). For cell suspensions from both lung and gut, **c**ollagenase action was antagonized with EDTA, and the remaining tissue was disrupted on a 100µm filter using a syringe plunger. Following centrifugation, cell pellets were subjected to red blood cell lysis (BioLegend) for 4 min, and cells

were resuspended in 2mL of PBS EDTA 2mM BSA 0,5%. Following excision, spleen samples were directly disrupted on a 100uM filter as for the lung samples, were treated for RBC lysis, and were finally resuspended in 2mL PBS EDTA 2mM BSA 0,1%. To prepare single cells from bone marrow, a set of femur and tibia was flushed by 10 ml RPMI containing 2% FCS and homogenized by pipetting for one minute. The resulting cell suspension was passed through a 70 μm strainer, treated for RBC lysis, and suspended in 2mL PBS EDTA 2mM BSA 0.1%.

Lung tissue preparation for single-cell RNA sequencing. Mouse lung cells were isolated from C57BL/6 as described above on day 0 (uninfected), day 1, day 3, and day 7 post-primary pneumonia, and from C57BL/6 mice on day 1, 3, and 7 after rechallenging. Cells were stained for 20 minutes with fixable viability eFluor7870 dye (Fisher Scientific). 300.000 viable single cells were FACS-sorted in PBS FCS 10% on a BD Aria IIu and processed for single-cell RNAseq protocol.

Cell encapsulation, single-cell libraries preparation, and sequencing for single-cell analysis CITE-seq, library preparation, and sequencing were carried out as previously described [50]. Briefly, cells Cells were counted, washed, and resuspended in 100µL Staining Buffer (PBS with 2% BSA and 0.01% Tween 20). Cells were incubated with 1µl anti-mouse CD16/CD32 for FcR blocking for 10 min in ice. 1µL of anti-mouse TotalseqA Hashtag oligonucleotide (HTO) antibody (Biolegend) were then added to each cell suspension with a unique hashtag sequence per time point and incubated on ice for 30 min (Table 1). Cells were washed three times 5 min in 1mL of Staining buffer at 500g. Cells were counted and pooled according to primary or secondary pneumonia. Cell viability of 67% was assessed on an ADAM cell counting instrument with Accu-chip kit. A total of 48,000 cells per pool were loaded in a Single-cell Chip A (reference PN-1000009) on a Chromium Next Controller (10x Genomics Inc. Pleasanton, CA). For the library preparation, we followed the Single Cell 3' v2 User Guide (version CG00052), applying several modifications. We adapted the Cell hashing protocol from the New York Genome Center Innovation Lab (Marlon Stoeckius & Peter Simbert) until the generation of cDNA and HTO libraries. In order to collect the HTO fraction at the clean-up step, we added 0.1µM of HTO Cell Hashing cDNA PCR additive primer (5'GTGACTGGAGTTCAGACGTGTGCTC) to the reaction mix for the first cDNA amplification step. Then we assigned PCR index with a unique i7 sequence to Gex and HTO libraries. See Table 2 for Single Index kit T Set A (PN-1000213) and Illumina TruSeq index assignment for cDNA Gex and HTO libraries, respectively.

This strategy was repeated once alongside cells isolated on day 1, day 3, and day 7 after a second bacterial infection in cured mice lungs. For each condition, 12,000 cells (with 90% viability) were loaded in a Single-cell Chip G (PN-1000120) on a Chromium Next Controller. Libraries were prepared following the version CG000206 Rev D of the Next GEM Single-cell 3' GEM v3.1 protocol with 3' feature barcoding technology for cell surface protein (PN-1000121 and PN-1000079). Results were integrated during data analysis (see below).

Cell preparation for TCRseq assay. Cells suspensions were prepared from three pooled uninfected, day 7, day 14 , and day 7 rechallenge lungs. 300,000 viable CD3+ CXCR6+ and CD3+ CXCR6- cells were FACS-sorted.

T cell encapsulation and TCRseq libraries preparation for TCR

CXCR6+ or CXCR6- T cells for day 0 (uninfected) or day 7 post-infection were processed as described for single-cell libraries preparation. Specifically for the preparation of single-cell TCR (scTCR) libraries and before the cell hashing, each cell suspension was incubated on ice for 20 min with a Totalseq C Hashtag and 1µL of a Biotin anti-mouse CXCR6 antibody coupled with Totalseq C anti-biotin PE (Table 3). At this point, we processed two technical replicates. The cell viability was assessed as described above and were 79% and 64% for both replicates. A total of 10,000 cells per replicate were then loaded on a Single-cell chip K (PN-1000286) on a Chromium Next Controller, and the preparation of VDJ, Gex, and Cell Surface libraries followed the Chromium Next GEM Single-cell 5' V2 protocol (version CG000330 Rev C) with 5' feature barcoding technology & Immune receptor mapping (PN-1000265 and PN-1000256) (Table 5).

Following the same protocol, we prepared scTCR libraries for CXCR6+ or CXCR6- T cells on day 14 post-infection or after a second bacterial infection in sepsis-cured mice lungs. 1uL of anti-mouse TCR γ/δ Totalseq C antibody (Biolegend) was added to the cells with unique Totalseq C Hashtags (Table 4). A total of 12,000 cells per replicates were loaded on a Chromium Next Controller, and VDJ, Gex, and Cell surface libraries were prepared (Table4). The cell viability of both replicates was 96% and 98%, respectively.

Next-Generation Sequencing of single-cell libraries.

300pM of pooled libraries were sequenced on a NovaSeq6000 instrument with an S1 100 cycles (v1.5) flow-cell kit (Illumina Inc. San Diego, CA). The programs were 29/8/0/101 cycles for sequencing scRNA libraries and 26/10/10/77 cycles for scTCR libraries.

Sequencing data analysis

Base calls were converted to read pairs and sorted according to libraries with Bcl2fastq2 9v2.20) (Illumina). No mismatches were allowed in the sequence of the indexes. The overall quality of the sequencing reads was assessed with FASTQC (v0.11.5)(The Babraham Bioinformatics group), and the reports were integrated with Multiqc (v1.12) [51]. No pre-processings of the sequencing reads were necessary.

After the read mapping against the reference genome GRCm38, the cells were called, and the unique molecular identifiers (UMI) were counted per gene with Cell Ranger Count for scRNAseq libraries (version 5.0.0, 10X Genomics) and Cell Ranger Multi for the scTCRseq libraries. The resulting raw expression was then processed with the R package Seurat (version 4.1.2) [52]. The first set of quality filters was applied. For further analyses, genes were considered if expressed in at least three cells. Cells expressing less than 200 detected genes and more than 5% sequencing reads mapped to mitochondrial genes were considered low-quality and thus removed. The raw expression values were log-normalized and hashtags corresponding to the time of sampling after infection were then demultiplexed with the function HTOdemux from Seurat package. Cells with over 4,000 detected genes or confidently associated with more than one hashtag were considered doublet and eventually removed. All scRNAseq data were integrated following the Seurat vignette defining a set of 2,000 anchor genes shared between the different datasets. Artifact correlations between gene expression were corrected by noise regularization [53], and for downstream analyses, a threshold of 0,1 was set on normalized expression.

Cell types were first inferred with the R package SCINA 9v1.2.0)[54], taking advantage of cell-type markers from the Panglao database [55]. This annotation of cell types was then manually refined. The cluster of Cxcr6+ cells was identified with differential expression analysis comparing multiple T cell clusters, and the significance was assessed with the Wilcoxon test. The concomitant expression of cytokine receptors in Cxcr6+ cells and cytokines in other immune cells was explored based on the KEGG pathway mmu:04060 “Cytokine-cytokine receptor interaction”[56], and the results were represented with the R package iTALK (Wang et al., preprint, bioRxiv). With the same rationale, further analyses of cell-cell communication were conducted with the R package CellChat (v1.1.3)[57]. Ligand-receptor interactions were considered when consistently observed in a minimum of 5 cells and with a p-value below 0.05.

The interferon signaling pathway was more deeply investigated with Interferome database [58] and the Interleukin signaling pathway with WikiPathways [59].

To compare the TCR repertoire between Cxcr6+ or Cxcr6- cells and uninfected or infected lungs, scTCRseq assays with different sampling time points were integrated with Cell Ranger Aggr (v5.0.0), and 200 cells for each condition were selected by random down-sampling. The TCR combinations of V, D, and J chains were further studied with VDJtools (v1.2.1)[60], computing statistics and comparing the different conditions. The transcriptomes of clonally selected or not selected Cxcr6+ cells were compared, defining two groups of cells based on clonotypes detected in a minimum of 4 cells.

Chromatin immunoprecipitation sequencing data for alveolar macrophages from uninfected and sepsis-cured C57BL/6 mice were issued from Roquilly et al. [12]. Data were re-analyzed as described previously [61]**, and genome browser tracks** were displayed based on normalized H3K27ac enrichment across the CXCL16 locus with IGV genome browser (v1.12.3)[62].

Resident T cells isolation and analysis. The following conjugated monoclonal antibodies were used on cell suspension (provided as name, clone, lot no., supplier and dilution): CD3-bv711, 145-2C11, 7311597, BD Biosciences, 1/200; CD4-alexaFluor 488, RM4-5, 4133940, BD Biosciences, 1/200; CD8-alexaFluor 700, RPA-T8, 9025745, BD Biosciences, 1/200; CD44-bv480, IM7, 8227752, BD Biosciences, 1/200; CD69-APC, H1.2F3, 9204727, BD Biosciences, 1/200; CD103-viobright515, REA789, 5191126445, Miltenyi, 1/100; CXCR6-PE/Dazzle594, SA203G11, B266429, BioLegend, 1/100; Fixable Viability Dye-eFluor 780, 2039434, eBioscience, 1:1,000; Ki67-bv421, B56, 8296617, BD Biosciences, 1/100; IL17-PE, eBio17B7, 4276914, eBioscience, 1/100; RORγt-bv421, Q31-378, 8151861, BD Biosciences, 1/100; TCRγδ-PeCy7, GL3, B291446, BioLegend, 1/200. Samples were acquired on an LSR-Fortessa or LSR-II (Becton Dickinson) and were analyzed using FlowJo software (TreeStar). Resident T cells were defined as $CD3^+$ $CD44^+$ $CD69^+$ cells on a viable single-cell lymphocyte gate.

In vivo antibody administration. Infected mice were intravenously injected with 10µg of CD45-PE on days 3 and 5 to evaluate T cell in vivo trafficking. Five minutes before the sample collection, 10µg of CD45-bv480 was intravenously injected to evaluate blood contamination during lung excision. To assess the CXCL16 role, CXCL16 antibody (142417, FHY0217111, R&D Systems, 50µg/mouse) or rat IgG2a isotype control was intravenously administrated in infected mice on days 4 and 6.

Adoptive cell transfers. For T cell adoptive transfers, splenic CD3+ cells were FACS-sorted (CD3-PE on single viable cells) from wt, *cxcr6*ko, or *ccr2*ko mice. For adoptive transfer of lung resident T cell, CD3+ CD44+ CD69+ cells were obtained from the lungs of wt or *cxcr6*ko mice 7-

days after sepsis. Purity above 95% was achieved, and 1x10^6 cells were intratracheally injected into Ly5.1 recipient animals. Resident T cells from donors were analyzed 36 hours later.

Lung metastasis. B16/F10 expressing ovalbumin (B16ova) and Lewis Lung carcinoma (LLC) cell lines were a gift from Louvet Cédric [63] and were maintained in culture in DMEM medium complemented with 10% fetal calf serum, penicillin-streptomycin, L-glutamine and sodium pyruvate and 7,5% sodium bicarbonate. B16ova and LLC were thawed three days before tail-vein administration (1x10^6 and 5x10^5 cells/mouse, respectively). Metastasis surface area and flow cytometry were performed 23 to 28 days following administration.

OT-I CD8 resident T cell generation. Naïve CD8+ lymphocytes from OT1 lymph nodes were magnetically purified (Miltenyi) and intravenously injected into Ly5.1 animals (2x10^5 cells/mouse) and ovalbumin was subsequently intratracheally administrated (200µg in 75µL PBS) to initiate ovalbumin specific CD8 resident T cells. *E. coli* pneumonia was induced 14 days after vaccination, and the ovalbumin challenge (200µg i.t. in 75µL PBS) was performed in sepsis-cured mice.

Immunofluorescence on human lung tumor samples.

Samples of human lung tumors were obtained from the tumor bank of CHU Nantes. The collection of human samples was declared to the French Ministry of Health authorization number DC 2011 – 1399) and was approved by an institutional review board. Written informed consent was obtained from patients before conservation. OCT-embedded Human tumors were snapped frozen, and 5 µm thick samples were fixed with 4% paraformaldehyde and permeabilized with 0.15% Triton-X100. Tissues were incubated with rat anti-mouse CD3 (CD3-12, GR3287379-3, Abcam, 1/200), rabbit anti-CXCR6 (polyclonal, 6466, Novus Biological, 1/200), primary antibodies, or corresponding isotype controls overnight at 4°C, followed by Alexa 488-conjugated donkey anti-rat IgG (polyclonal, 2092264, Invitrogen, 1/200) and Alexa 568-conjugated donkey anti-rabbit IgG (polyclonal, 2136776, Invitrogen, 1/200) respectively for one hour. Slides were mounted in Prolong Diamond antifade mounting medium with DAPI (Invitrogen) for nuclei counterstaining. Slides were observed under a Zeiss AxioImager Z2 microscope with AxioVision Release 4.8.2 (06-2010) software (Carl Zeiss). Fields were recorded at the 20x objective N.A. 0,45. Images were analyzed using Fiji Is Just ImageJ software (version 1.53c, Java 1.8.0_172, National Institutes of Health, Bethesda, MD, USA).

Statistical analysis. Data were plotted using a GraphPad prism. An unpaired *t*-test with two-tailed *P* values and 95% confidence intervals was used. One-way analysis of variance (ANOVA) with

Bonferroni correction (posthoc tests) was used for multiple comparisons. A linear regression test investigated correlations. The figure legends can find statistical details of experiments (exact number of mice per group, exact *P* values, dispersion, and precision measures). $P < 0.05$ for statistical significance.

Definitions of human TRM gene signatures from the literature

Human lung tumor TRM gene signature was defined from the publicly available datasets (GSE83637 [31,32]) by selecting the significantly up-regulated genes (with LFC >2 and adjusted p-value <0.01) from lung tumor TRM versus lung tumor non-TRM samples (JEM_20190249_TableS4.xlsx). Lung TRM signature was defined by selecting significantly up-regulated genes from normal lung TRM versus normal lung non-TRM samples (JEM_20190249_TableS2.xlsx). Dermis TRM signature was defined by selecting significantly up-regulated genes from dermis TRM vs. dermis non-TRM (JEM_20190249_TableS3.xlsx (Clarke, 2019). To have a non-overlapping set of genes for each signature, the common genes were removed in the following manner:

$$\boldsymbol{CXCR6} = FPKM\ expression\ of\ the\ CXCR6$$
$$\boldsymbol{tumour_{TRM}} = tumuor'_{TRM} - \{lung'_{TRM} \cup \boldsymbol{CXCR6}\}$$
$$\boldsymbol{lung_{TRM}} = lung'_{TRM} - \{tumour'_{TRM} \cup \boldsymbol{CXCR6}\}$$
$$\boldsymbol{dermis_{TRM}} = dermis'_{TRM} - \{\boldsymbol{tumour_{TRM}} \cup \boldsymbol{lung_{TRM}}\}$$

TCGA Datasets analyses

Tissue-specific GDC TCGA RNA-Sequencing and corresponding survival clinical data were obtained from the UCSC website (https://xenabrowser.net/datapages/). Non-tumor samples were removed following the TCGA sample ID convention. The normalized FPKM values were log-transformed with $log_2(FPKM + 1)$ transformation. The signature score for a given set of genes from bulk RNAseq for TCGA and human lung tumor data was computed following the approach described by Keerthivasan et al. [64]. The values for each log transformed gene were first z-transformed across all samples. The resulting z-scores were then averaged across genes to arrive at a single signature score for each sample. Pearson correlation coefficient was used for gene correlations. The t-test was used for computing significance, and a p-value of less than 0.05 was considered statistically significant. For survival analysis of TCGA data, the survival cutoff for patients was set as 'low' with a percentile expression of ≤ 0.33 and as 'high with a percentile expression ≥ 0.66. The R modules survfit and ggsurvplot were used for the Kaplan Meier survival plots.

Cross-projections of tissue-resident T cell gene signatures.

For human TRM T cell gene signature, gene expression was computed for 7 patients with a paired sample of $CD8^+CD103^+$ TRM / $CD8^+CD103^-$ non-TRM T cells (from EGAS00001004707 [33]). Unique transcript.versionID was matched with the HGNC symbol using the mapping information available at https://uswest.ensembl.org/biomart/martview to convert human genes to mice genes. The counts of duplicate gene symbols were aggregated by taking their sum. The human tumor TRM gene signature set was then derived from the differential gene expression analysis of CD8+CD103+ TRM vs CD8+CD103- non-TRM population. This differential gene expression (DGE) analysis was performed with DESeq2 R package with the design argument set to account for patient+population.

The definition of the tissue resident T cells gene signature from sepsis-cured mice was developed by performing DEG analysis using FindMarkers on mouse data with Cxcr6 T cells versus all other cells from the sc-RNA-seq data with $avg\_\log_2 FC > 2$ and $p\_val\_adj < 0.05$. The gene signature score was computed using Seurat's AddModuleScore function. Common DEG from all tested days were retained to define an alternative tissue resident T cells signature geneset.

For the cross-projections, the mice orthologues of human genes were found from the mapping information available on the biomart website. The human homologous of mice TRM geneset was obtained from the mapping information available on the biomart website. The same mapping information was used to reverse map the mice gene orthologues for the TRM geneset identified from the human T cell infiltrating lung tumor data or the TRM genesets (see above). All other downstream analyses were performed using Seurat.

Data availability

Single-cell sequencing data supporting this study's findings have been deposited in ENA with the PRJEB52332 accession code (https://www.ebi.ac.uk/ena/browser/home).

Figs. S1 to S11

Tables S1 to S2

Figure 1

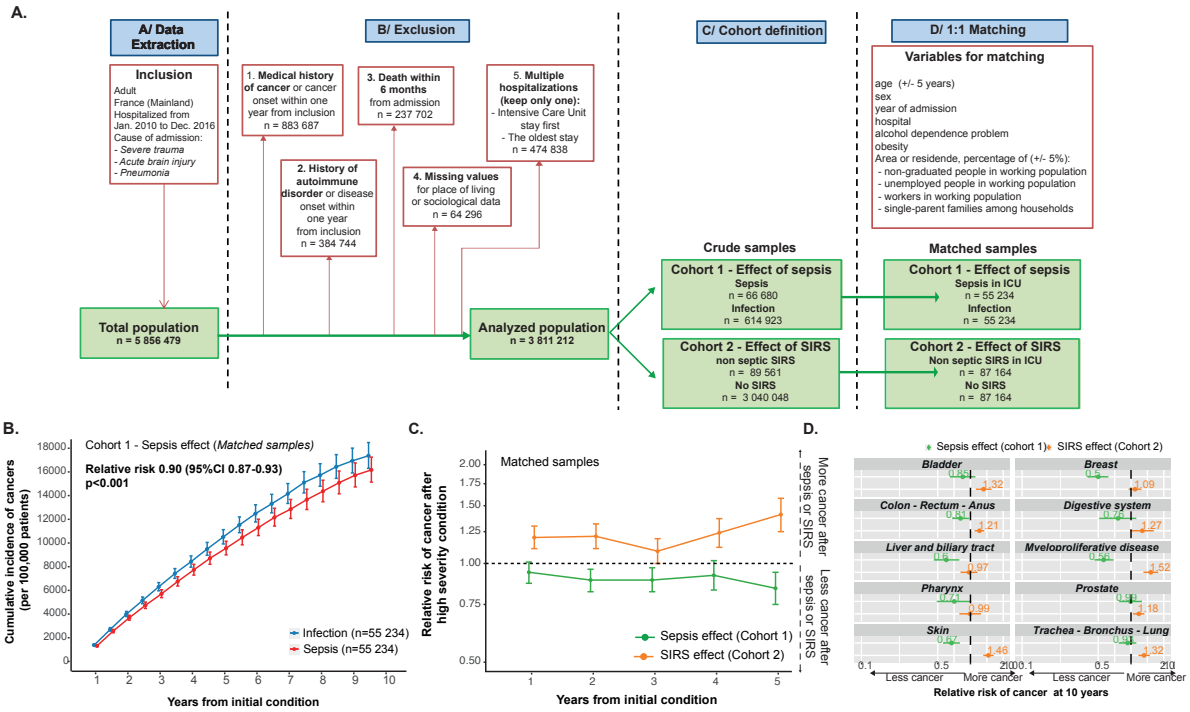

Figure 1. Decreased risk of cancer up to ten years after cure from sepsis in humans
(A) Flow chart of the crude and matched nationwide French cohort 1 (Sepsis effect) and cohort 2 (non-septic SIRS effect) with a 10-year follow-up. **(B)** Cumulative incidences of cancers in sepsis survivors and infection survivors after ten years of follow-up in the matched sample of cohort 1. Curves represented as calculated incidence ± SD. **(C)** Instantaneous relative risk (RR) of cancer in sepsis vs. matched infection survivors (green line) and non-septic SIRS vs. no SIRS (orange line) at the indicated time after the index medical condition. RR > 1 means increased risk in the severe condition, and a RR < 1 means a reduced risk of cancer. **(D)** Relative risk of the ten most frequent cancer localizations in sepsis vs. infection survivors (green line) and non-septic SIRS vs. no SIRS (orange line) at the indicated time after the index medical condition. RR > 1 means increased risk in the severe condition, and a RR < 1 means a reduced risk of cancer.

Figure 2

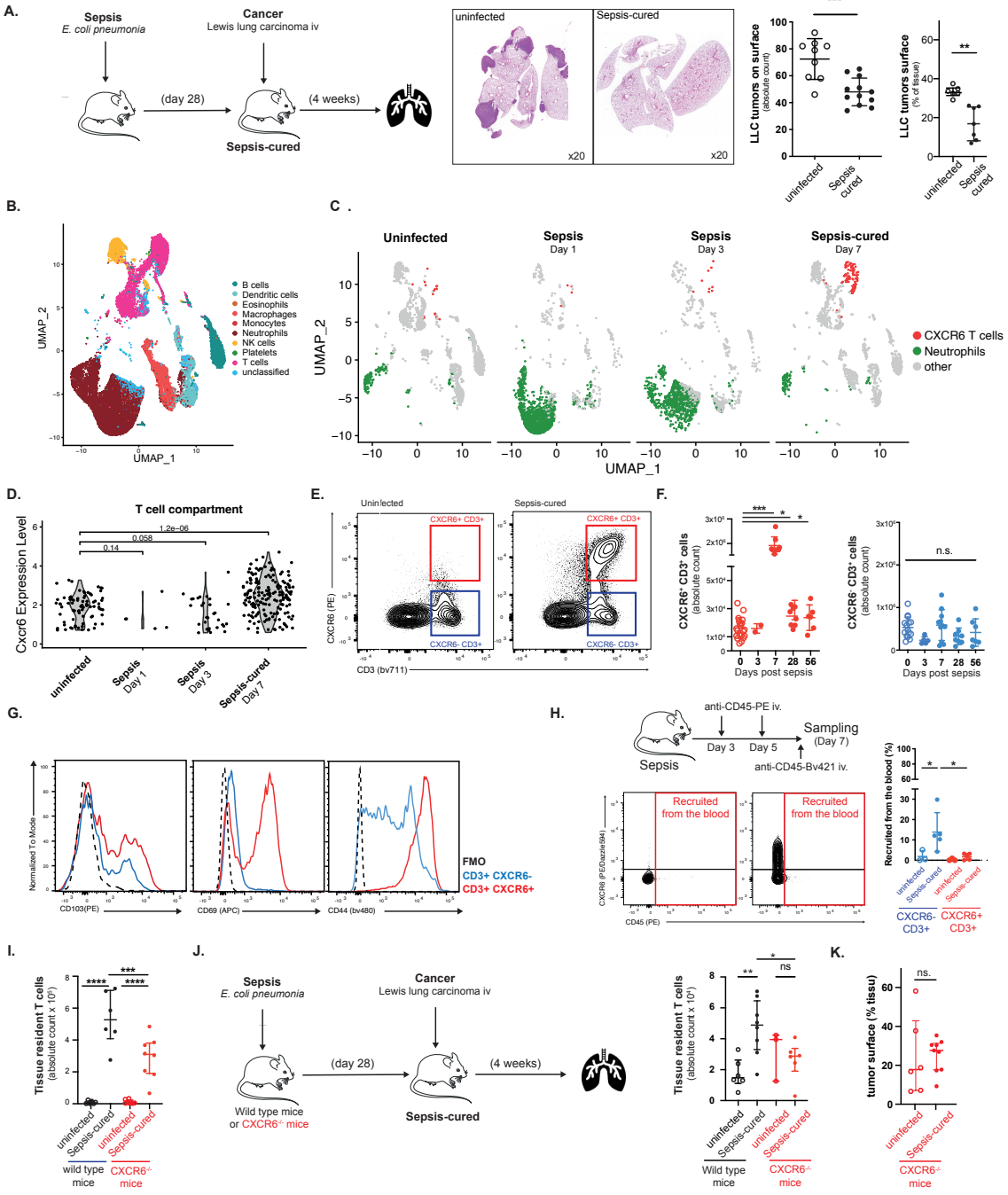
A.
Sepsis
E. coli pneumonia
Cancer
Lewis lung carcinoma iv
(day 28)
(4 weeks)
Sepsis-cured
uninfected
Sepsis-cured
x20
x20
LLC tumors on surface
(absolute count)
LLC tumors surface
(% of tissue)
uninfected
Sepsis cured
B.
UMAP_1
UMAP_2
B cells
Dendritic cells
Eosinophils
Macrophages
Monocytes
Neutrophils
NK cells
Platelets
T cells
unclassified
C .
Uninfected
Sepsis
Day 1
Sepsis
Day 3
Sepsis-cured
Day 7
CXCR6 T cells
Neutrophils
other
D.
T cell compartment
Cxcr6 Expression Level
1.2e−06
0.058
0.14
uninfected
Sepsis Day 1
Sepsis Day 3
Sepsis-cured Day 7
E.
Uninfected
Sepsis-cured
CXCR6+ CD3+
CXCR6- CD3+
CXCR6 (PE)
CD3 (bv711)
F.
CXCR6+ CD3+ cells
(absolute count)
CXCR6- CD3+ cells
(absolute count)
n.s.
Days post sepsis
G.
Normalized To Mode
CD103(PE)
CD69 (APC)
CD44 (bv480)
FMO
CD3+ CXCR6-
CD3+ CXCR6+
H.
Sepsis
anti-CD45-PE iv.
Day 3
Day 5
Sampling
(Day 7)
anti-CD45-Bv421 iv.
Recruited from the blood
CXCR6 (PE/Dazzle594)
CD45 (PE)
Recruited from the blood (%)
CXCR6- CD3+
CXCR6+ CD3+
I.
Tissue resident T cells
(absolute count x 10⁴)
wild type mice
CXCR6-/- mice
J.
Sepsis
E. coli pneumonia
Cancer
Lewis lung carcinoma iv
(day 28)
(4 weeks)
Wild type mice
or CXCR6-/- mice
Sepsis-cured
Tissue resident T cells
(absolute count x 10⁴)
Wild type mice
CXCR6-/- mice
K.
tumor surface (% tissu)
CXCR6-/- mice

Figure 2. The increase in CXCR6$^+$ tissue-resident memory T cells reduces the cancer growth in sepsis-cured mice.

(A) Respiratory sepsis was induced by intra-tracheal instillation of *E. coli*. LLC was injected iv. in uninfected and sepsis-cured mice (infected 28 days prior), and the number and surface of lung metastasis were investigated 4 weeks after. Graphs represent median ± IQR pooled from 3 independent experiments (n=9 for uninfected, =12 for the count in sepsis-cured, and =7 for tumor surface in sepsis-cured). **(B)** UMAP representing the immune cell compartment in mouse lung annotated from the scRNA-seq. 10,542 single cells from 2 mice from all time points were analyzed. (**C)** UMAP representation of the immune cell type distribution across time points. **(D)** Time course of the expression level of Cxcr6 in the T cell clusters. **(E)** Representative plots of CD3 and CXCR6 expressions measured by flow cytometry of single cells obtained after enzymatic digestion of the lung tissue harvested in uninfected and *E. coli* lung sepsis-cured mice (representative of more than 10 mice/group). **(F).** Numbers of CXCR6$^+$ CD3$^+$ cells and CXCR6$^-$ CD3$^+$ cells in the lungs at the indicated time point (n=6 to 10 mice per time point). Graphs represent median ± IQR and are pooled data from 3 independent experiments.**(G).** Expressions of classical markers of tissue-residency on CXCR6$^+$ and CXCR6$^-$ CD3$^+$ cells of sepsis-cured mice. Representative of 3 independent experiments (n > 10 mice per group). **(H)** PE-conjugated anti-CD45 antibody was injected intravenously 3 and 5 days after *E. coli* sepsis. Brilliant Violet PE (BV)420 conjugated anti-CD45 antibody was injected immediately before sampling to remove T cells adherent to the endothelium. The percentages of blood recruited (BV420$^-$ PE$^+$) CXCR6$^-$ and CXCR6$^+$ T cells were measured on day 7 (n=5 mice per group). Graph represents median ± IQR and is pooled data from 2 independent experiments. **(I)** Number of tissue-resident T cells in wild type and Cxcr6-deficient mice uninfected or infection cured. Graphs represent median ± IQR and are pooled data from 2 independent experiments. (n=6 for wild-type groups, and = 8 for Cxcr6-deficient groups). **(J)** LLC was injected in wild-type and Cxcr6-deficient (Cxcr6$^{-/-}$) mice cured of *E. coli* lung sepsis. The number of tissue-resident T cells was investigated 4 weeks after. (n=6 uninfected WT, =8 sepsis-cured WT, =3 uninfected Cxcr6$^{-/-}$ mice, =6 for sepsis-cured CXCR6$^{-/-}$ mice). Graphs represent median ± IQR and are pooled data from 3 independent experiments. **(K)** LLC were injected in wild-type and Cxcr6-deficient (Cxcr6$^{-/-}$) mice cured of *E. coli* lung sepsis. The surface of lung metastasis was investigated 4 weeks after. Graphs represent median ± IQR and are pooled data from 2 independent experiments. (n=6 for uninfected and =9 for sepsis-cured CXCR6$^{-/-}$ mice).

Statistical significance was assessed by the Mann-Whitney test (**A**), Wilcoxon test **(D),** and a One-way analysis of variance with Bonferroni correction was used for multiple comparisons (**F, H, I, K,**).*P ≤ 0.05, **P ≤ 0.01, ***p<0.001.

Figure 3

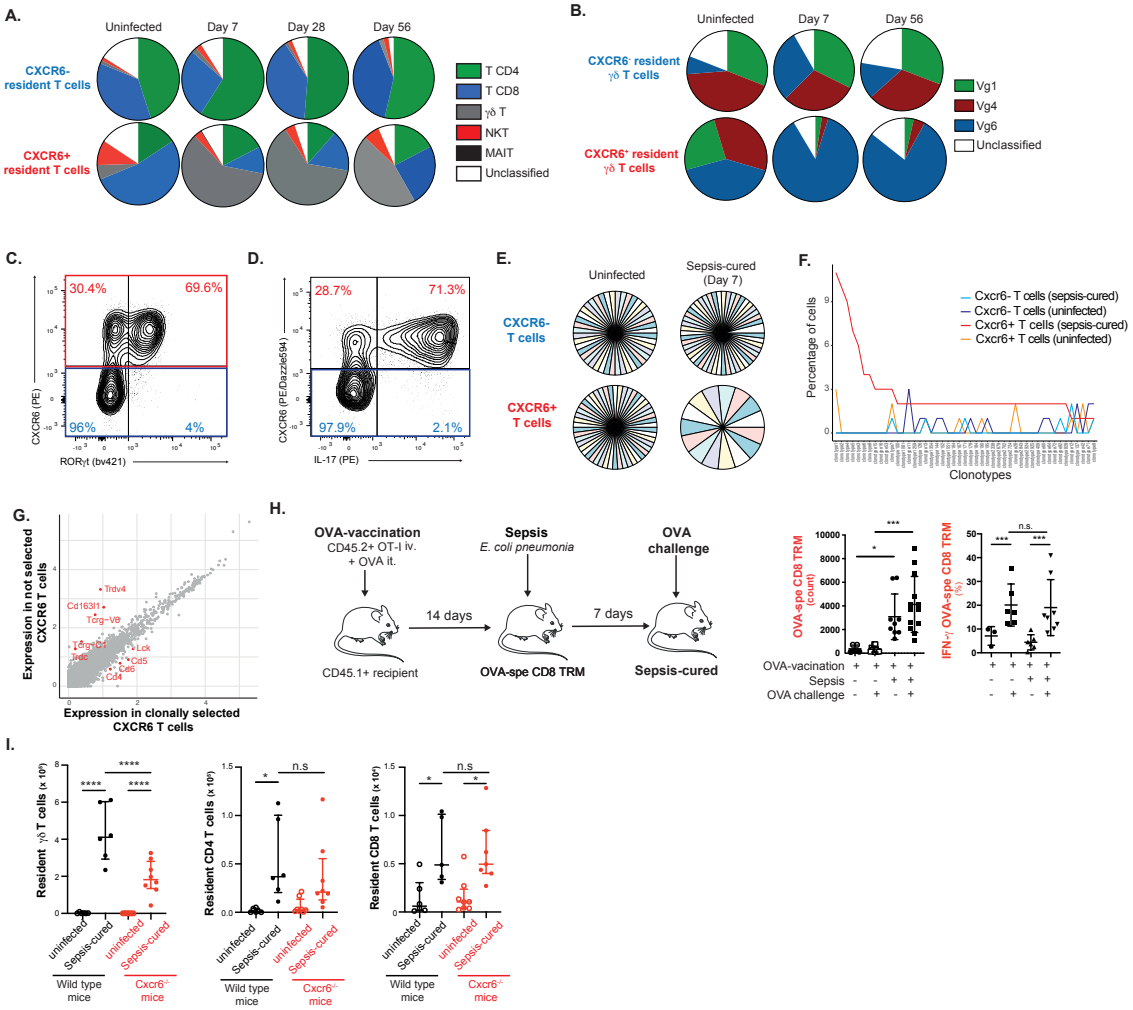

Figure 3. CXCR6$^+$ IL17$^+$ Vγ6δ T cells decrease tumoral growth after sepsis

(A) Percentages of CD4$^+$, CD8$^+$, MAIT, γδ T cells, NK1.1$^+$, MAIT, and unclassified cells among resident CXCR6$^+$ and CXCR6$^-$ CD3$^+$ cells at the indicated time point of sepsis (n = 6 mice/group at each time point). Pi-charts represent median ± IQR and are pooled data from 3 independent experiments. **(B)** Pi-charts illustrating the distribution of Vγ1, Vγ4, and Vγ6 chains in resident CXCR6$^-$ and CXCR6$^+$ γδ T cells in uninfected or sepsis-cured (day 7 or day 56) mice. (n=6 mice/group). Data are pooled data from 2 independent experiments. **(C-D)** Frequencies of RORγt$^+$ (C) and IL-17$^+$ (D) cells among CXCR6$^+$ CD3+ cells in sepsis-cured mice (representative of 6 mice). **(E)** Pi-charts illustrating the distribution of TCRV-β families in CXCR6$^+$ T cells in uninfected or sepsis-cured (day 7) mice. (n=4 mice/ group). Data are pooled data from 2 independent experiments. **(F)** Frequency of the top 20 TCR clonotypes in CXCR6$^+$ and CXCR6$^-$ T cells in uninfected or sepsis-cured (day 7) mice. (n=4 mice/ group). Data are pooled data from 2 independent experiments. **(G)** Test for differential gene expression between clonally selected CXCR6$^+$ T cell (clonotype represented in at least 4 cells) and non-clonally selected (clonotypes found in only cell) CXCR6+T cells. Significantly differentially expressed genes were highlighted in red. (n = 4 mice/group). Data are pooled data from 2 independent experiments. Each group is

composed of 82 cells. **(H)** CD45.2$^+$ OT-I cells (iv) and OVA (intra-tracheal) were injected 14 days before the *E. coli* lung sepsis induction in CD45.1$^+$ recipient mice. Production of IFNγ by CD45.2$^+$ OVA-specific and CD45.1$^+$ non-OVA specific tissue-resident CD8 T cells in response to OVA intratracheal instillation was determined 7 days later. (n = 10-12 mice/group). Data are pooled data from 3 independent experiments. **(I)** Number of resident γδ, CD4 and CD8 T cells in uninfected and septic-cured wild-type and Cxcr6-deficient mice. (n = 6 wild-type mice and =8 Cxcr6-deficient mice). Graphs represent mean ± SD and are pooled data from 3 independent experiments. Statistical significance was assessed by one-way analysis of variance with Bonferroni correction used for multiple comparisons (H, I). *P ≤ 0.05, **P ≤ 0.01, ***P ≤ 0.001, ****P ≤ 0.0001

Figure 4

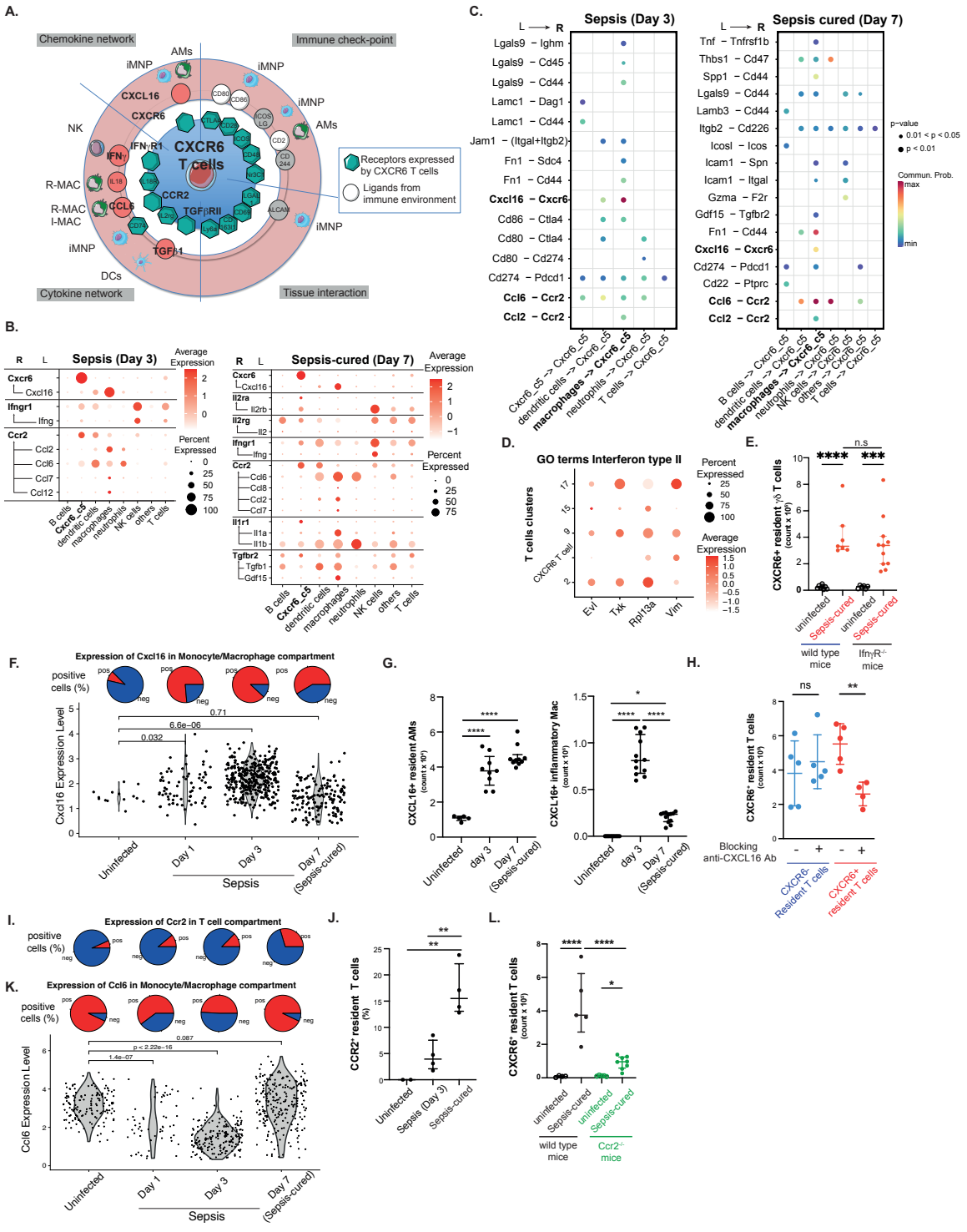

Figure 4. Local chemokines and cytokines networks expand tissue-resident CXCR6 γδ T cells after sepsis

(A) Receptor-ligands (R-L) network in the lungs of uninfected and sepsis-cured mice developed by systematic literature research of known R-L interactions. **(B)** Expression of cytokine receptors

on CXCR6 T cells and cognate cytokines in the different cell type compartments during (left panel) and after (right panel) sepsis. Pairs of cytokine and cytokine receptors were initially extracted from the KEGG database. The colors represent the average expression level, and the circle radius represents the percentage of expressing cells. **(C)** R-L map in the lung during (left panel) and after (right panel) sepsis. Communication probability between CXCR6 T cells expressing receptors (R) and other cell types expressing cognate ligands (L). Both receptors and ligands were expressed in a minimum of 5 cells, and the curated lists of mouse-specific receptors and ligands were provided by the R package CellChat. Communication probabilities with p-values ≤ 0.05 were considered significant. (**D)** Expression of the interferon type II pathway effector genes in the T cell compartment. The colors represent the cell-cell communication probability for each test R-L and the circle radius the significance. **(E)** Number of resident CXCR6$^+$ γδ T cells in uninfected and sepsis-cured wild-type and IfnγR deficient mice. (n =7 wild-type and 11 IfnγR deficient mice per group). Graphs represent median ± IQR and are representative of 2 independent experiments. **(F)** Percentages of Cxcl16 expressing cells (pi-charts, n = 2 mice per time point) and Cxcl16 RNA expression levels (boxplots) in the monocytes/macrophages cluster at the indicated time point after *E. coli* pneumonia. The ratio of positive (red) and negative (blue) cells is represented in the upper panel. (n = 2 mice per time point). **(G)** Number of CXCL16$^+$ resident alveolar macrophages and inflammatory macrophages at the indicated time point after *E. coli* pneumonia. (n = 5 mice per group). Graphs represent median ± IQR and are pooled from 2 independent experiments. **(H)** Number of tissue resident CXCR6+ T cells in sepsis-cured mice treated on day 3 and day 5 with blocking anti-CXCL16 antibody or isotype control. (n = 4-5 mice per group). Graphs represent median ± IQR and are representative of 2 independent experiments. **(I)** Pi-charts representing percentages of *Ccr2* expressing cells in the T compartment at the indicated time point. (n = 2 mice per time point). **(J)** Percentages of CCR2$^+$ tissue-resident T cells measured by flowcytometry at the indicated time after lung sepsis. (n = 2 uninfected and 4 mice during sepsis and sepsis-cured). Graphs represent median ± IQR from one experiment. **(K)** Pi-charts represent percentages of *Ccl6* expressing cells and *Ccl6* expression levels in the monocytes/macrophages compartment at the indicated time point. The ratio of positive (red) and negative (blue) cells is represented in the upper panel. (n = 2 mice per time point). **(L)** Number of tissue resident CXCR6$^+$ T cells in wild-type and Ccr2-deficient mice either uninfected or 7 days after sepsis. Graphs represent median ± IQR and are pooled data from 2 independent experiments. (n=5 for wild-type groups, and = 8 for Ccr2-deficient groups). Statistical significance was assessed by the Wilcoxon rank sum test (**F, J**), Mann-Whitney test (**H**), and one-way analysis of variance with Bonferroni correction was used for multiple comparisons (**G, K**).*P ≤ 0.05, **P ≤ 0.01, ***p<0.001.

Figure 5

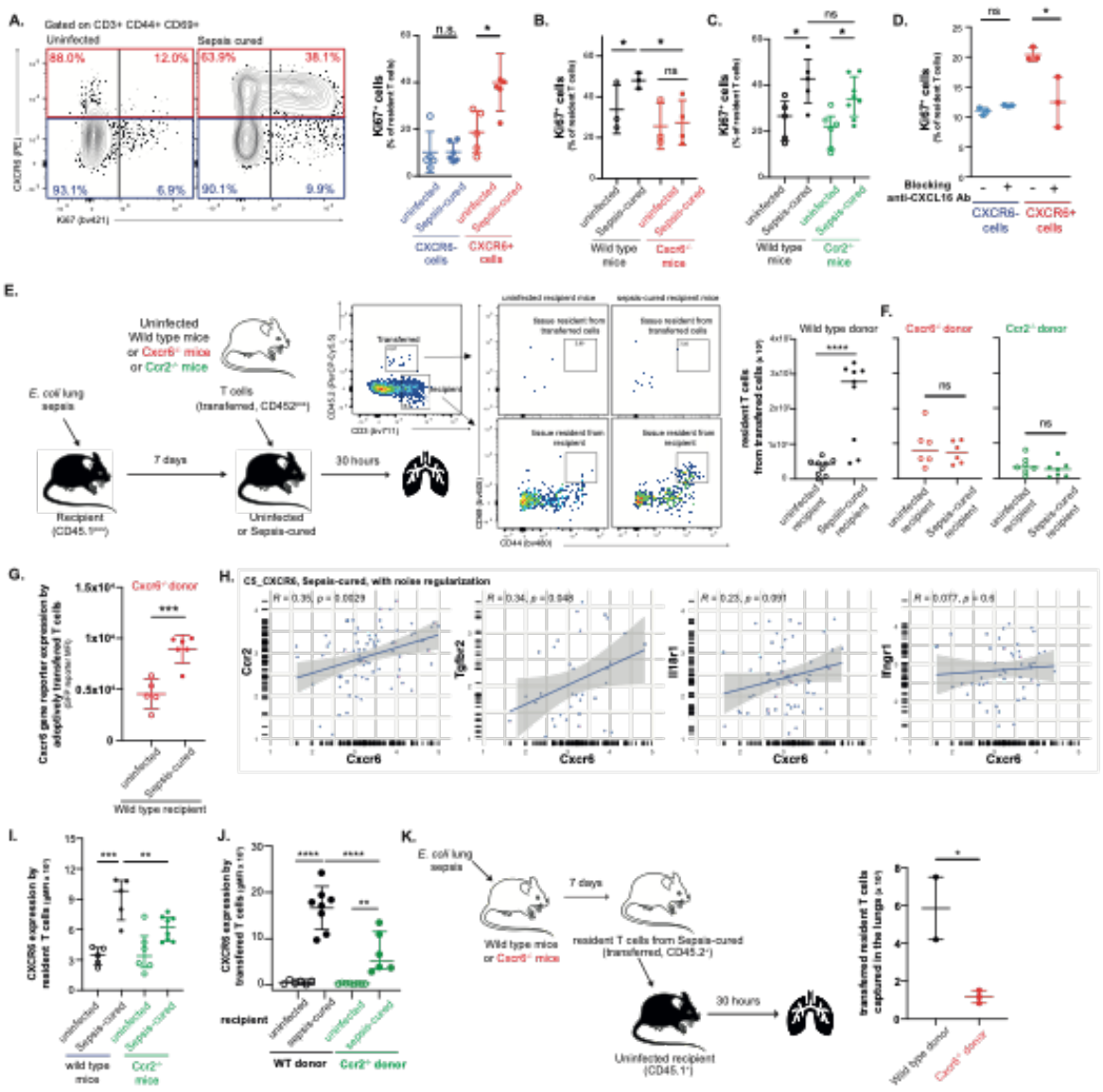

Figure 5. Post-septic lung niche increases the tissue residency of proliferating γδ T cells via a CCR2-dependent upregulation of CXCR6 expression.

(A) Representative plots and frequencies of Ki67^{+} cells in CXCR6^{+} and CXCR6^{-} resident T cells in uninfected and sepsis-cured mice. (n=5 mice/group). Graphs represent median ± IQR and are pooled data from 2 independent experiments. **(B-C).** Frequencies of Ki67^{+} cells among resident T cells in uninfected and sepsis-cured (B) Cxcr6-deficient or (C) Ccr2-deficient mice (n=5 mice/group). Graphs represent median ± IQR and are pooled data from 2 independent experiments. **(D).** Frequencies of Ki67^{+} cells in CXCR6^{+} and CXCR6^{-} resident T cells in uninfected and sepsis-cured mice treated on day 3 and day 5 blocking anti-CXCL16 antibody or isotype control. (n=3 mice/group). Graphs represent median ± IQR and are pooled data of 2 independent experiments. **(E-F).** Recipient mice (CD45.1^{pos}) were infected with *E. coli,* and seven days later, they were intratracheally injected with T cells collected from uninfected (E) wild type or (F) Cxcr6-deficient

or Ccr2-deficient donors (CD45.2^{pos}). The number of resident T cells issued from transferred cells was measured 36 hours later in the lungs of the recipient (n = 9 wild-type mice/condition, 6 Cxcr6-deficient mice/condition, and 7 Ccr2-deficient mice/condition). Graphs represent median ± IQR and are pooled data from 3 independent experiments. **(G).** Expression of the GFP under the control of *Cxcr6* promoter after adoptive transfer of Cxcr6-deficient T cells in the lungs of uninfected or sepsis-cured recipients (n = 5-6 mice per group). Graphs represent median ± IQR and are pooled data from 2 independent experiments. **(H)** Pearson correlations of the stated receptor gene expressions with *Cxcr6* gene expression in *Cxcr6* tissue-resident T cells in sepsis cured mice. **(I).** CXCR6 membrane expression on tissue-resident T cells of uninfected or sepsis-cured wild type or Ccr2-deficient mice (n = 5 wild type mice/condition and 7 Ccr2-deficient mice/condition). Graphs represent median ± IQR and are pooled from 2 independent experiments. **(J)** CXCR6 expression by Ccr2-deficient T cells after adoptive transfer in the lungs of uninfected or sepsis-cured recipients (n = 8 wild type/condition mice and =6-8 Ccr2-deficient mice/condition). Graphs represent median ± IQR and are pooled data from 2 independent experiments. **(K)** Resident T cells collected from sepsis-cured wild-type or Cxcr6-deficient donors (CD45.2^{pos}) were intratracheally injected in uninfected wild-type mice (CD45.1^{pos}). The number of transferred cells in the lungs of the recipient was measured 30 hours later (n = 2 wild-type donors and =4 Cxcr6-deficient donors). Graph represents median ± IQR issued from 1 experiment.

The correlation was tested by the Pearson test (**G**), and statistical significance was assessed by the Mann-Whitney test (**D-F, J**) or one-way analysis of variance with Bonferroni correction was used for multiple comparisons (**A-C, H**). *P ≤ 0.05, **P ≤ 0.01, ***P ≤ 0.001, ****P ≤ 0.0001.

Figure 6

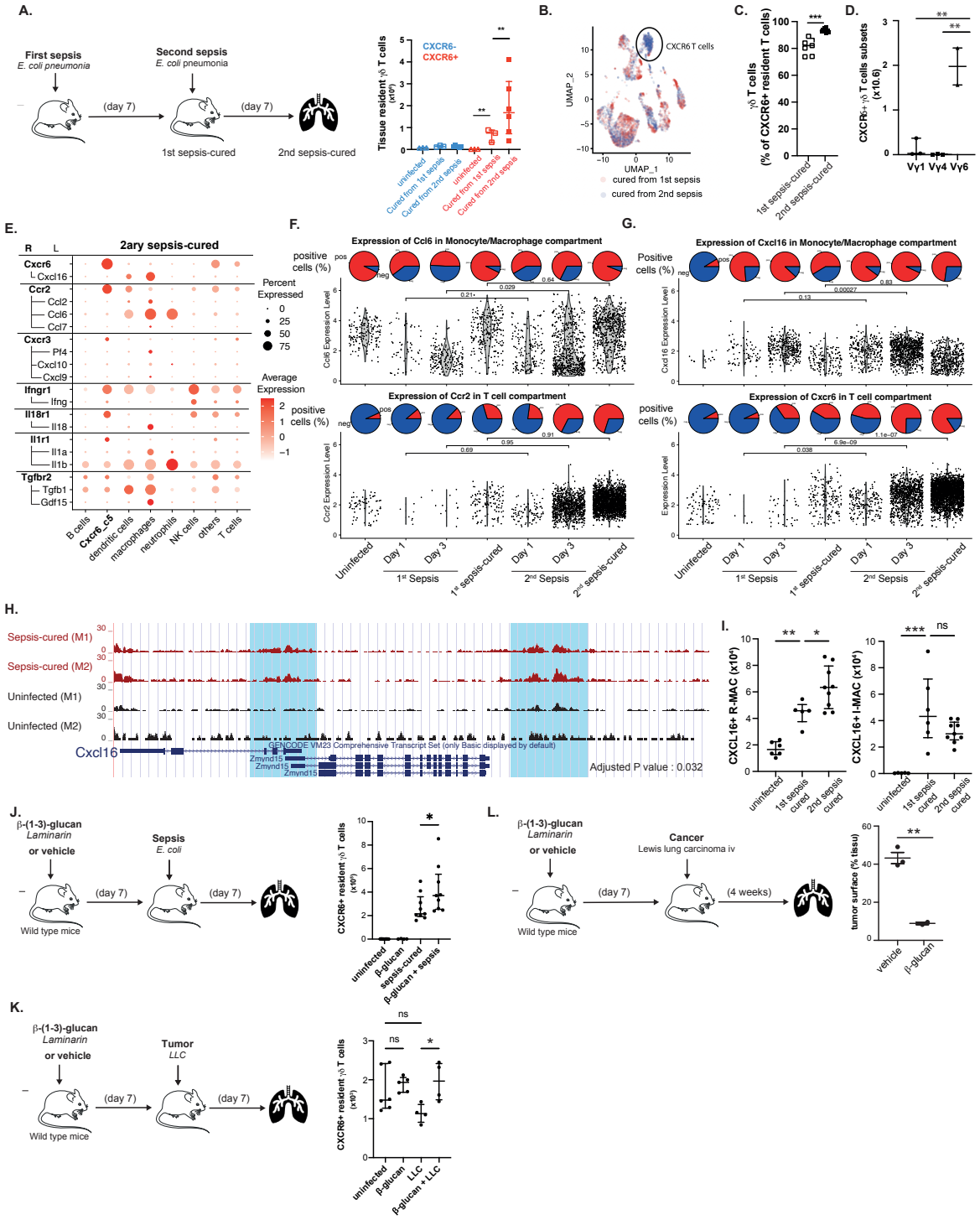

Figure 6. Epigenetic regulation increases the ability of macrophages to induce residency of γδ t cells during secondary immune challenge

(A) Number of CXCR6^{-} or CXCR6^{+} tissue-resident T cells in uninfected, first-sepsis cured, or secondary sepsis cured mice (n = 3 uninfected, =3 primary sepsis-cured and =6 secondary sepsis-cured). Graph represents median ± IQR and is pooled from two independent experiments. **(B)**

UMAP of cell clusters obtained by sc-RNA sequencing of lung immune cells ($CD45^+$) in first-sepsis (red) or secondary (red) sepsis-cured mice (n=2 independent biological replicate per condition). **(C)** Percentages of γδ T cells among CXCR6 resident T cells in primary-sepsis or secondary-sepsis cured mice (n=7 mice/group). Graph represents median ± IQR and is pooled of two independent experiments. **(D)** Numbers of CXCR6+ Vγ1, Vγ4, Vγ6 δ T cells in secondary sepsis cured mice (n=3 mice/group). Graph represents median ± IQR and is pooled of two independent experiments. **(E)** Expression of cytokine receptors on CXCR6 T cells and cognate cytokines in the different immune cell type compartments of mice cured from secondary sepsis. The colors represent the average expression level, and the circle radius represents the percentage of expressing cells. Pairs of cytokine and cytokine receptors were initially extracted from the KEGG database. (**F)** Pi-chart representing percentages of *Ccl6* expressing cells and *Ccl6* expression levels in the monocytes/macrophages cluster (top) and *Ccr2* expressing cells in the T clusters (bottom) at the indicated time point after primary and secondary sepsis. (n = 2 independent biological replicate per time point). **(G)** Pi-chart representing percentages of Cxcl16 expressing cells and Cxcl16 expression levels in the monocytes/macrophages cluster (top) and Cxcr6 expressing cells in the T clusters (bottom) at the indicated time point after primary and secondary sepsis. (n = 2 independent biological replicate per time point). (**H)** Genome browser of median H3K27 acetylation of the gene locus corresponding to Cxcl16 in resident alveolar macrophages of uninfected (black) or sepsis-cured (red) mice. **(I)** Number of CXCL16+ resident alveolar macrophages in first and secondary sepsis cured mice. (n=5 first sepsis-cured and 9 secondary sepsis-cured). Graph represents median ± IQR and is pooled of two independent experiments. **(J-K)** Mice were treated with β-(1-3)-glucan (laminarin, i.p.) or vehicle, and the number of CXCR6 tissue-resident γδ T cells was determined (J) after sepsis-cure or (K) during LLC development. (n=3 mice for laminarin alone, =9 mice for sepsis-cured mice, =5 mice for LLC). Graph represents median ± IQR and is pooled of two independent experiments. **(L)** Mice were treated with laminarin (i.p.) or vehicle, then injected with LLC (i.v.) 7 days later. The lung tumor surface was measured 4 weeks later. (n=3 mice for vehicle and 2 for laminarin). Graph represents median ± IQR and is pooled of two independent experiments. Statistical significance was assessed by a Mann-Whitney test (D, L), Wilcoxon test (G and H), one-way analysis of variance with Bonferroni correction was used for multiple comparisons (A-B, E, J-K). *$P \leq 0.05$, **$P \leq 0.01$, ***$P \leq 0.001$.

Figure 7

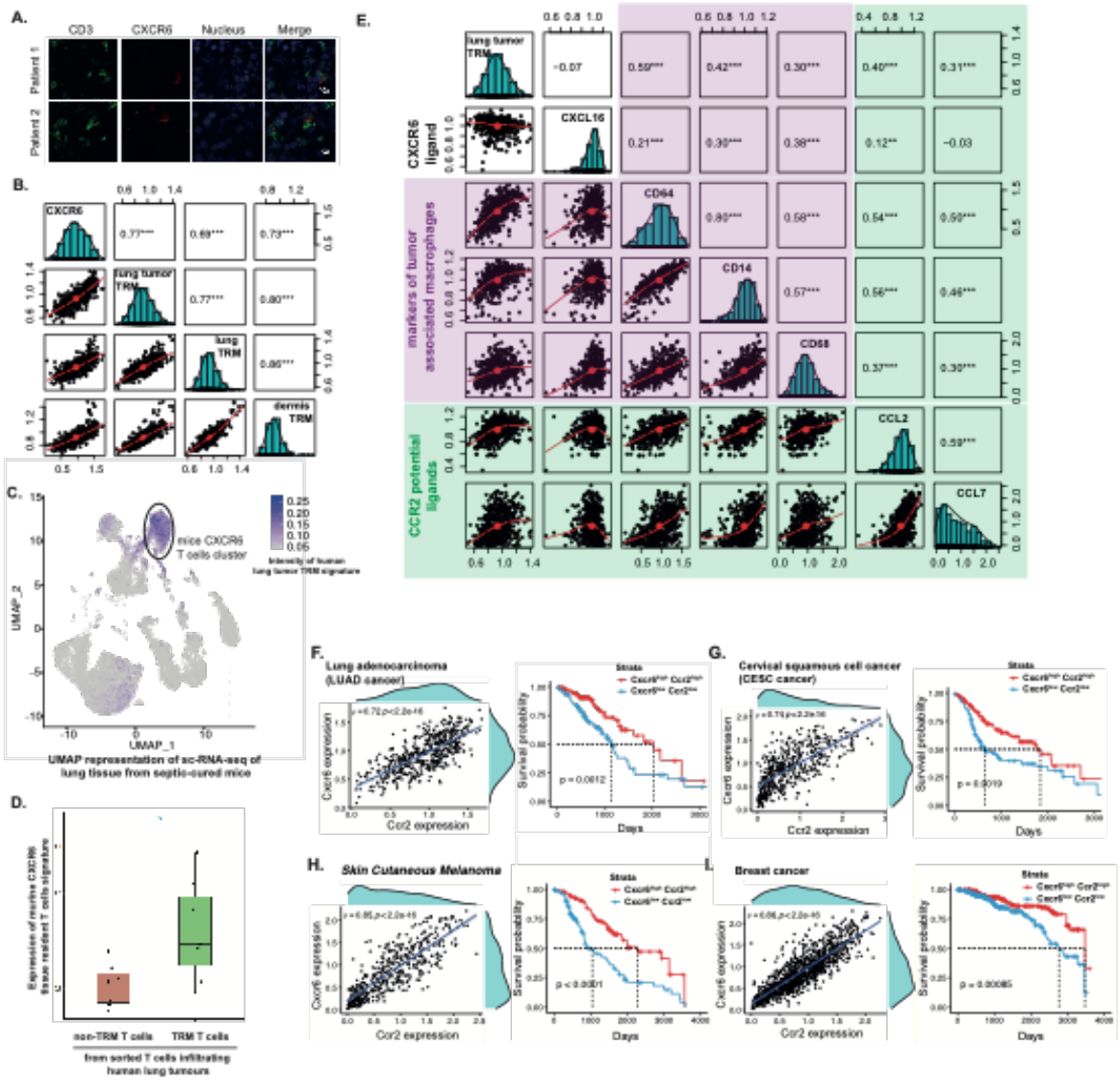

Figure 7. CCR2 CXCR6 co-expression predicts survival in human cancer patients

(A) Immunostained sections two human lung cancer. Representative of 4 patients. Green: CD3, Red: CXCR6, Blue: DAPI. **(B)** Correlation between CXCR6 level and lung tumor TRM, lung TRM, and dermis TRM gene signatures from publicly available datasets GSE111898 [31] for lungs and GSE83637 [32] for the dermis. **(C)** Projection of the gene signature of human tissue-resident T cells infiltrating lung tumor (from EGAS00001004707 [33]) on the UMAP representation of single-cell RNA-seq of lung tissue from septic-cured mice. **(D)** Level of expression of the murine CXCR6 tissue-resident T cells signature in TRM vs. non-TRM T cells infiltrating human lung cancer (from EGAS00001004707 [33]). (n=7 patients). **(E)** Correlation between lung tumor TRM gene signature, Cxcl16, macrophage markers (CD64, CD14, CD68), and potential CCR2 ligands (Ccl2, Ccl7) from LUAD cancer (TCGA database). **(F)** Co-expression of CXCR6 and CCR2; and Kaplan-Meier estimates of overall survival of lung adenocarcinoma (LUAD) patients stratified by scores

Co-expression of CXCR6-CCR2. P-values are based on the univariate Cox proportional-hazards model (high versus low). Tick marks indicate censoring (death or loss of follow-up). **(G-I)** As in (E) for cervical squamous cell cancer (F), cutaneous skin melanoma (G), and breast cancer (H).

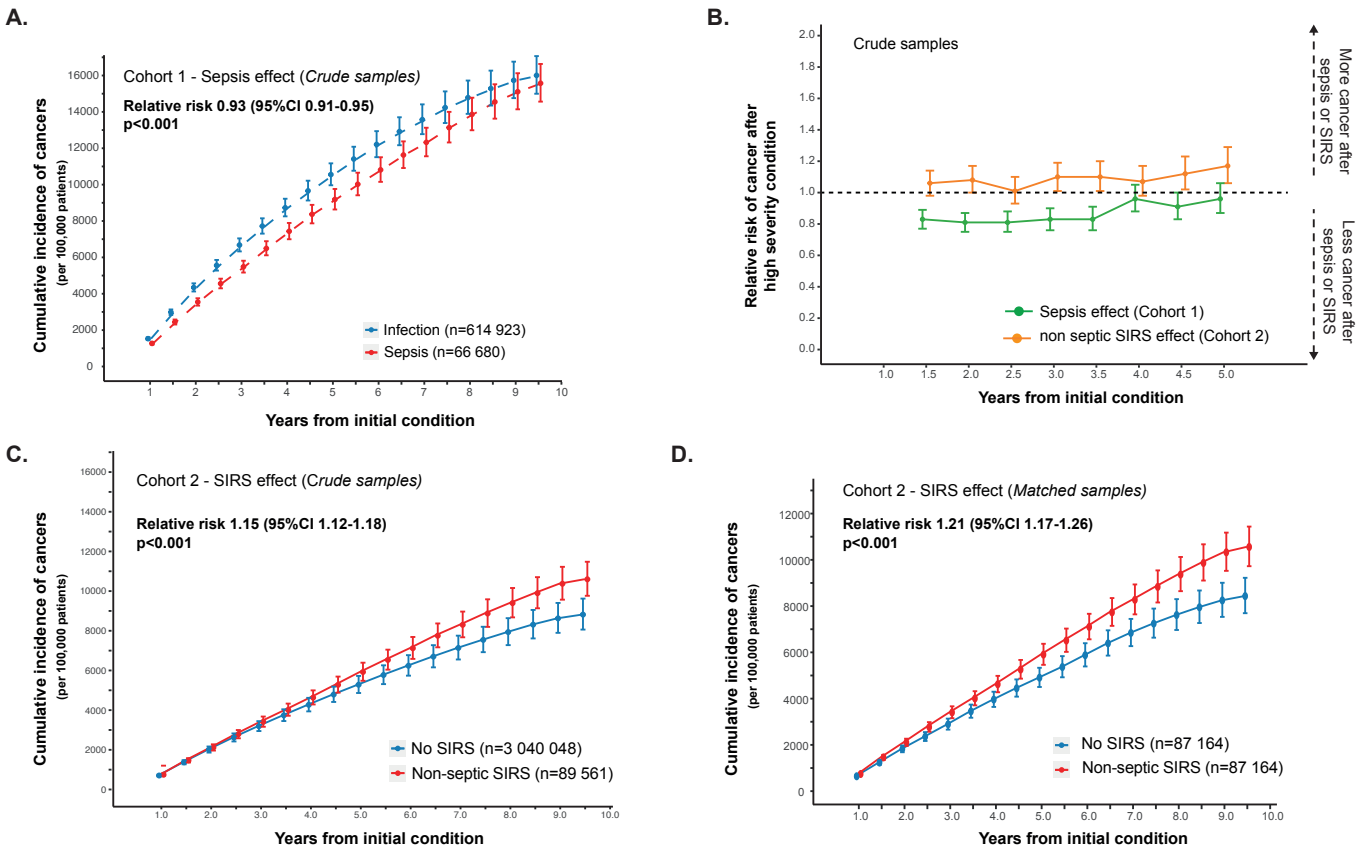

Figure S1

A. Cumulative incidences of cancers in sepsis survivors and infection survivors after ten years of follow-up in the crude sample of cohort 1. Curves represented as calculated incidence +/- SD.

B.Relative risk (RR) of cancer in sepsis vs. infection survivors (green line) and non-septic SIRS vs. no SIRS (orange line) at the indicated time after the index medical condition. RR > 1 means increased risk in the severe condition, and a RR < 1 means a reduced risk of cancer. Results were obtained in the matched samples of cohorts 1 and 2.

C-D. Cumulative incidence of cancers in non-septic SIRS and no-SIRS survivors after ten years of follow-up in the (C) crude and (D) matched samples. Curves represented as calculated incidence +/- SD.

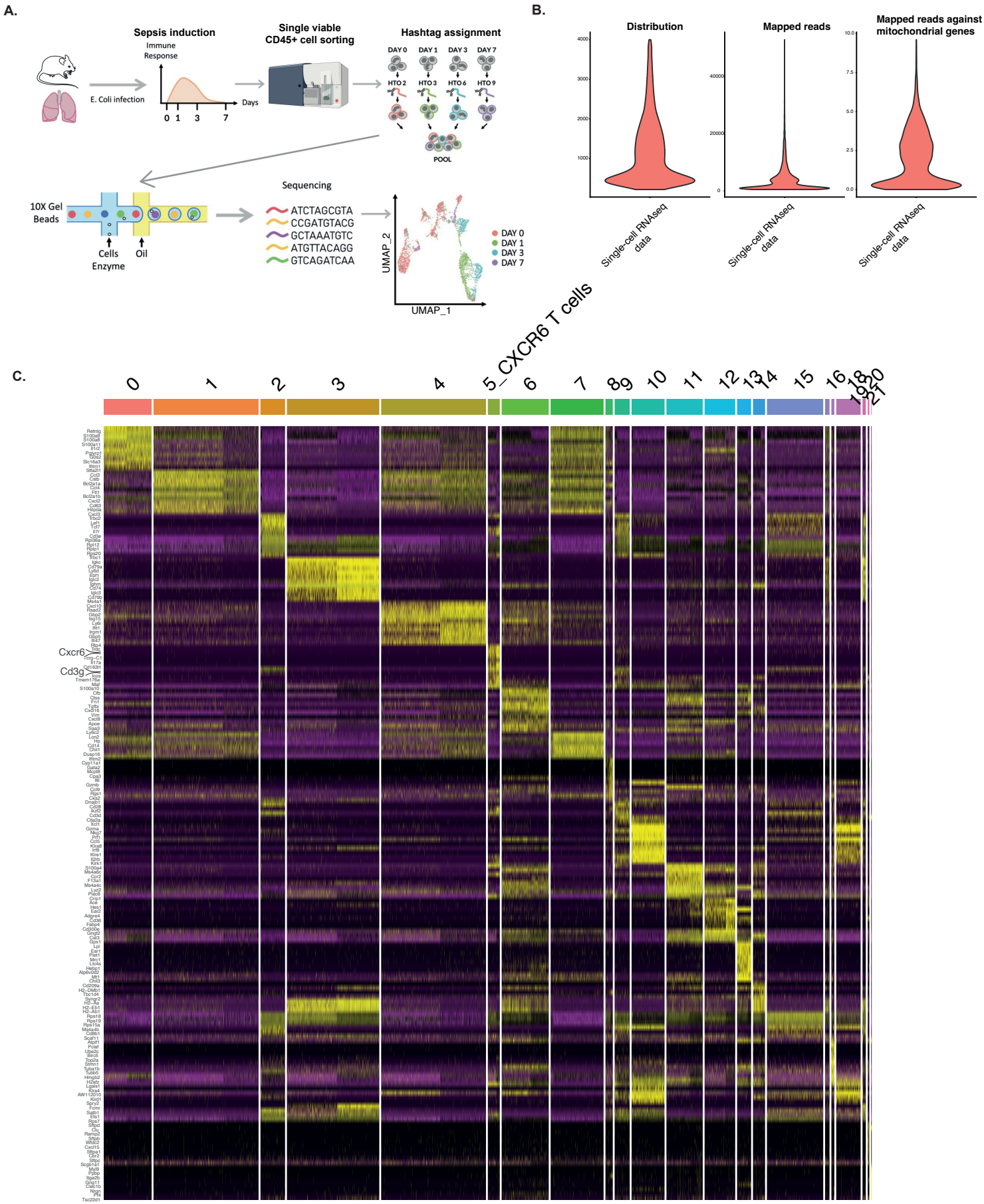

Figure S2

A. Rationale of single-cell RNA sequencing assay.

B. Quality controls of the single-cell RNA sequencing data representing the distribution of detected genes (left panel), mapped reads (middle panel), and reads mapped against mitochondrial genes (right panel) per cell.

C. Heatmap of top 10 markers per cluster. Cxcr6 and Cd3g are characteristic of cluster 5.

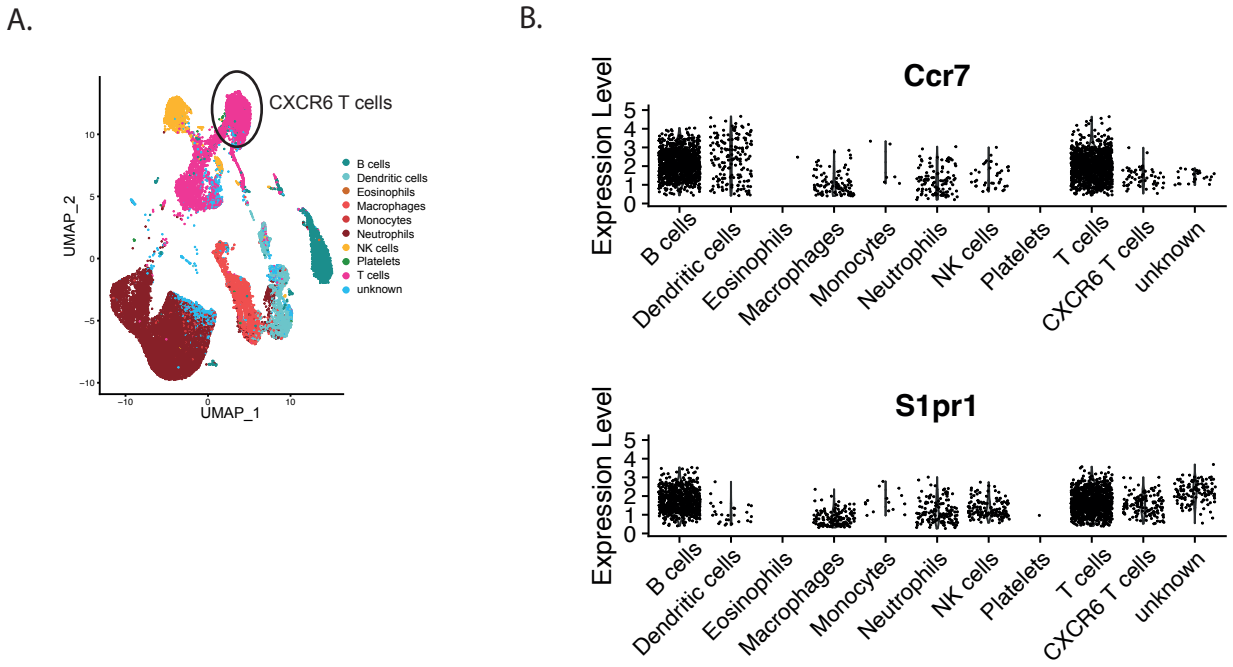

Figure S3

A. Clustering (numbers) and annotation (colors) of immune cells from the scRNAseq in mouse lung.

B. Expression of Ccr7 (top) and S1pr1 (bottom) in immune cells of mice lung.

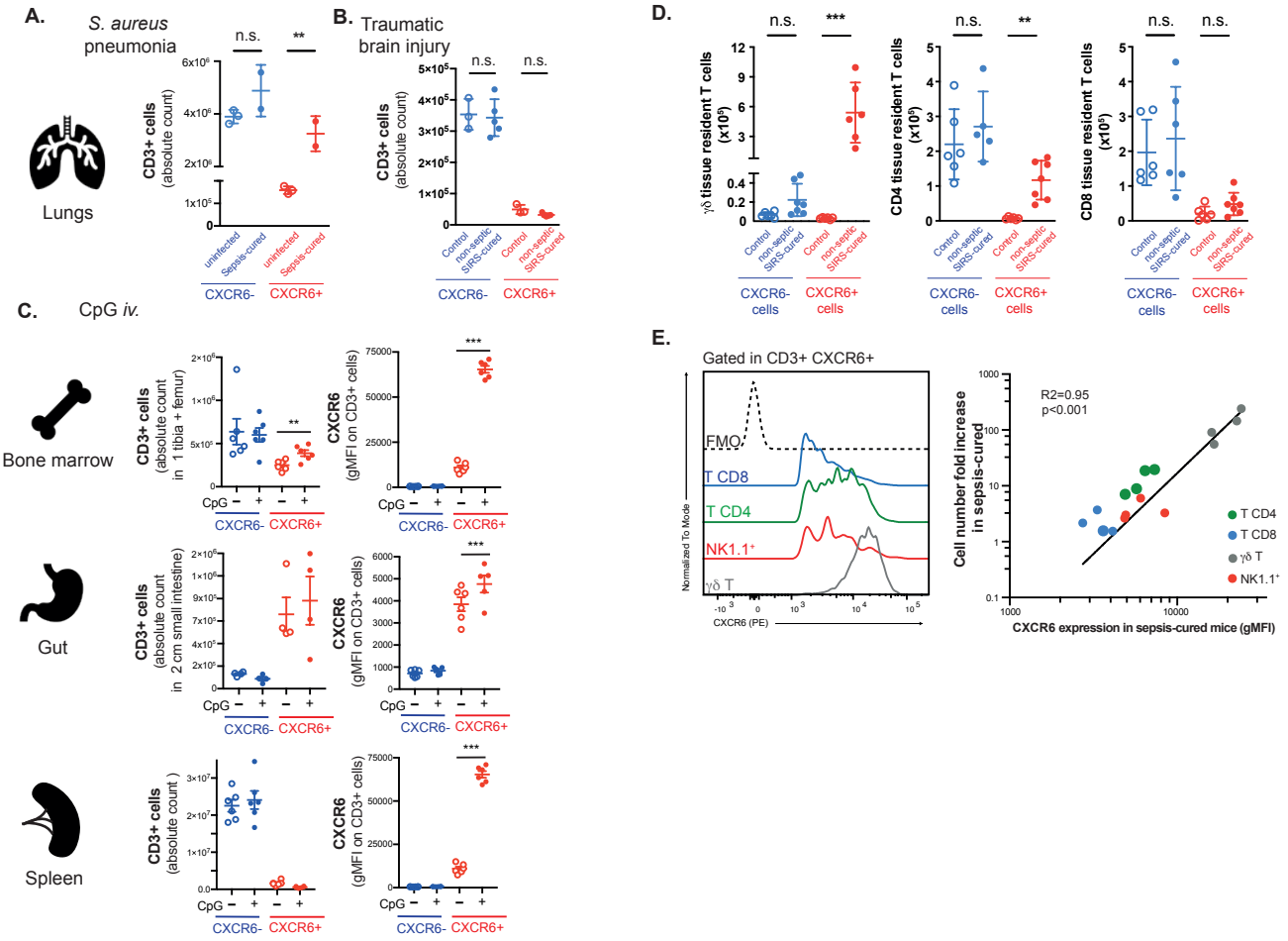

Figure S4

A. Numbers of CXCR6- CD3+ and CXCR6+ CD3+ cells in the lungs 7 days after S. aureus sepsis (n=2-3 mice per time point). Graph represents median ± IQR from a single experiment.

B. Numbers of CXCR6- CD3+ and CXCR6+ CD3+ cells in the lungs 7 days after traumatic brain injury (n=3-5 mice per time point). Graph represents median ± IQR from a single experiment.

C. Numbers of CXCR6- CD3+ and CXCR6+ CD3+ cells in the bone marrow, the gut, and spleen 7 days after CpG i.v. Administration (n=6 mice per time point). Graph represents median ± IQR, pooled data from 2 independent experiments.

D. Number of CXCR6- and CXCR6+ tissue resident T cells in uninfected and sepsis-cured mice. (n=6 mice per time point). Graph represents median ± IQR, pooled data from 2 independent experiments.

E. Expression of CXCR6 on CD8, CD4, NK1.1+ and T cells (left panel) and linear regression of T cell subsets increase and their CXCR6 expression in 7 days infection-cured mice (right panel).

Statistical significance was assessed by Mann-Whitney tests (A-C), and Correlation was tested by the Pearson test (D). *P ≤ 0.05, **P ≤ 0.01, ***P ≤ 0.001.

Figure S5

A-B. Expression of genes associated with the Wikipathway «Chemokine signaling» (WP2292) during (A) and after (B) sepsis. The color gradient represents the level of expression, and the circle radius the percentage of expressing cells.

A. Sepsis (Day 3)

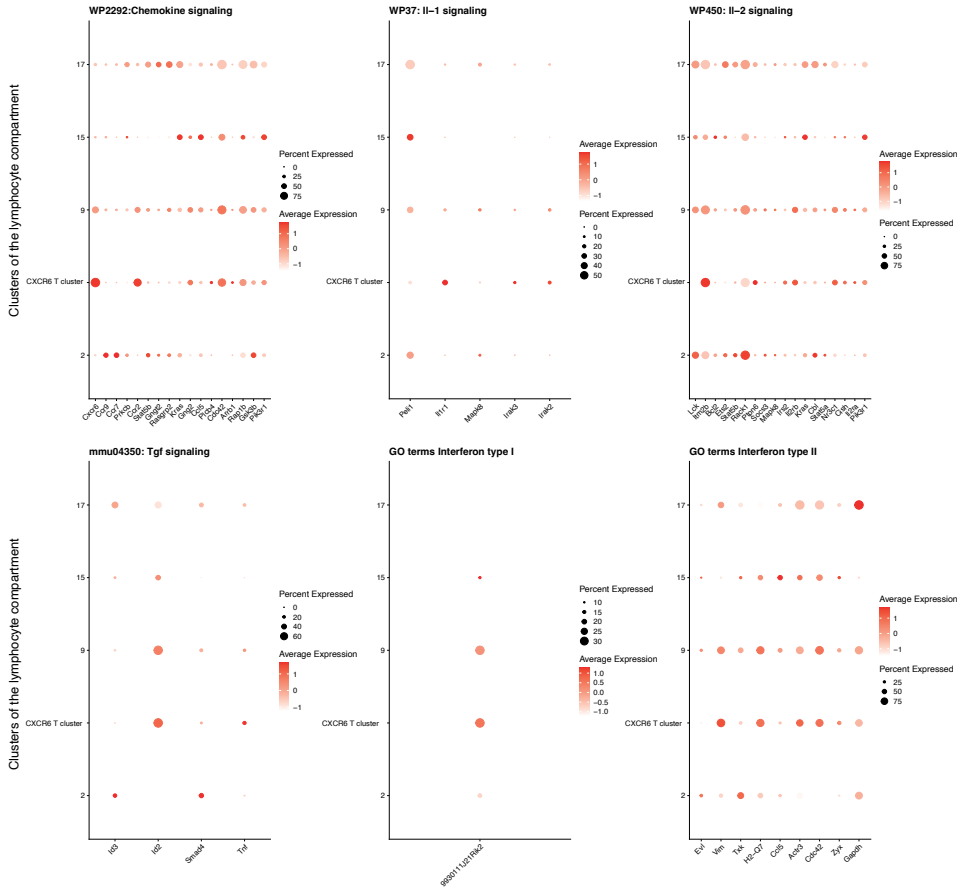

B. Sepsis-cured (Day 7)

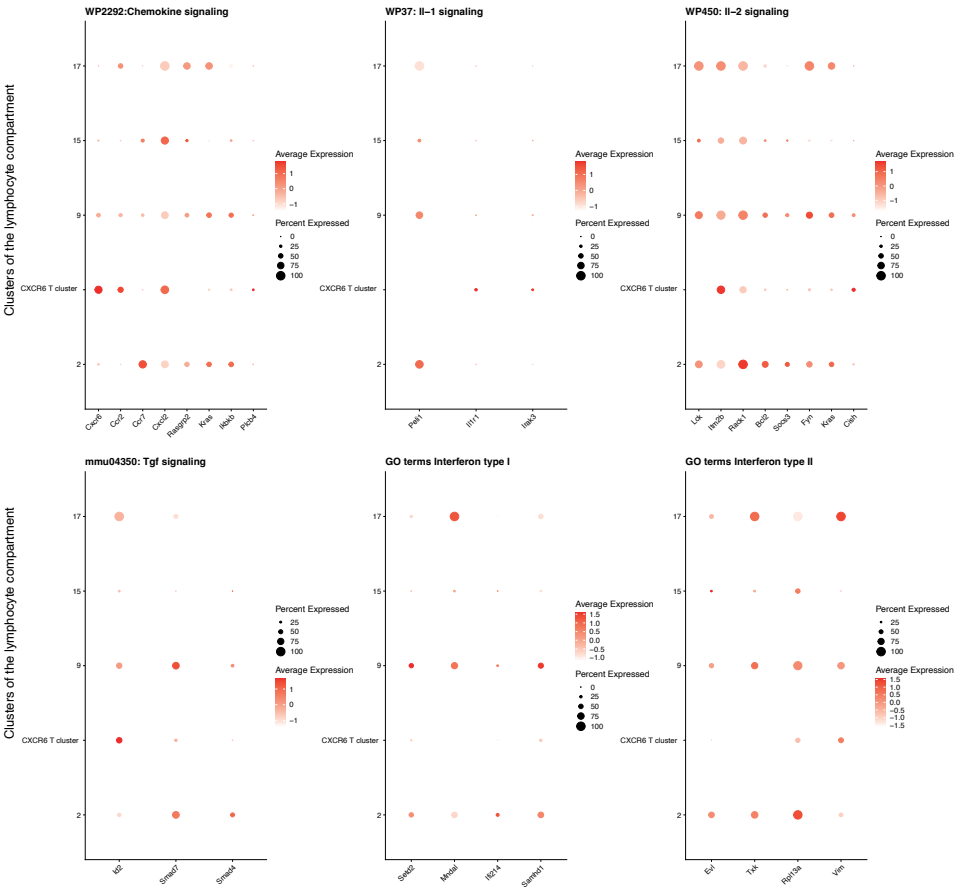

Figure S6

A-B. Expression of cytokine and chemokine signaling genes in the T cell compartment during (A) and after (B) sepsis. The color gradient represents the level of expression, and the circle radius the percentage of expressing cells.

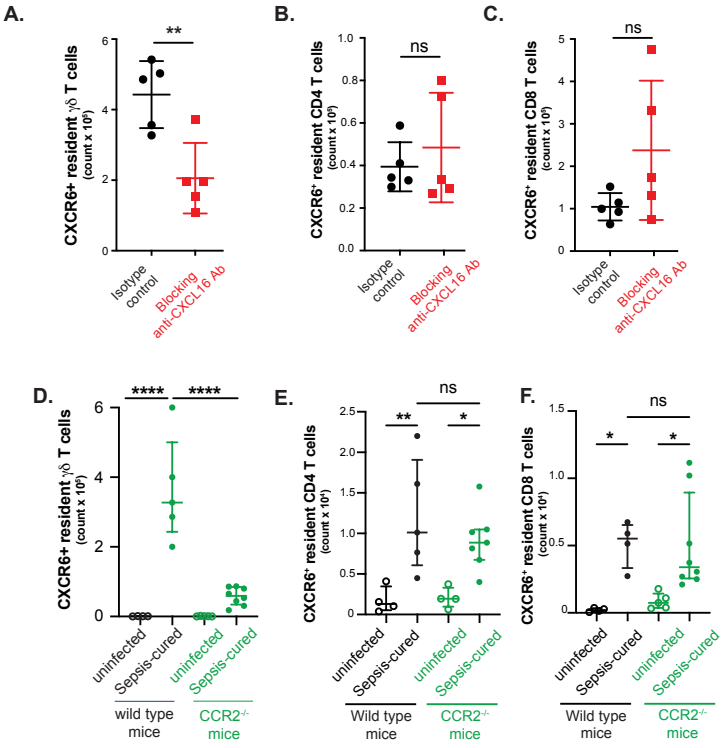

Figure S7

A-C. Numbers of tissue-resident CXCR6+ (A) γδ, (B) CD4 and (C) CD8 T cells in sepsis-cured mice treated on day 3 and day 5 blocking anti-CXCL16 antibody or isotype control. (n = 5 mice per group). Graphs represent median ± IQR and are pooled data of 2 independent experiments.

D-F. Number of tissue-resident CXCR6+ (D) γδ, (E) CD4, (F) CD8 T cells in uninfected and sepsis-cured wild-type and Ccr2-deficient mice. (n = 5-7 mice /group). Graphs represent median ± IQR and are pooled data of 2 independent experiments. Statistical significance was assessed.

One-way analysis of variance with Bonferroni correction was used for multiple comparisons.
*P ≤ 0.05, **P ≤ 0.01, ***p<0.001.

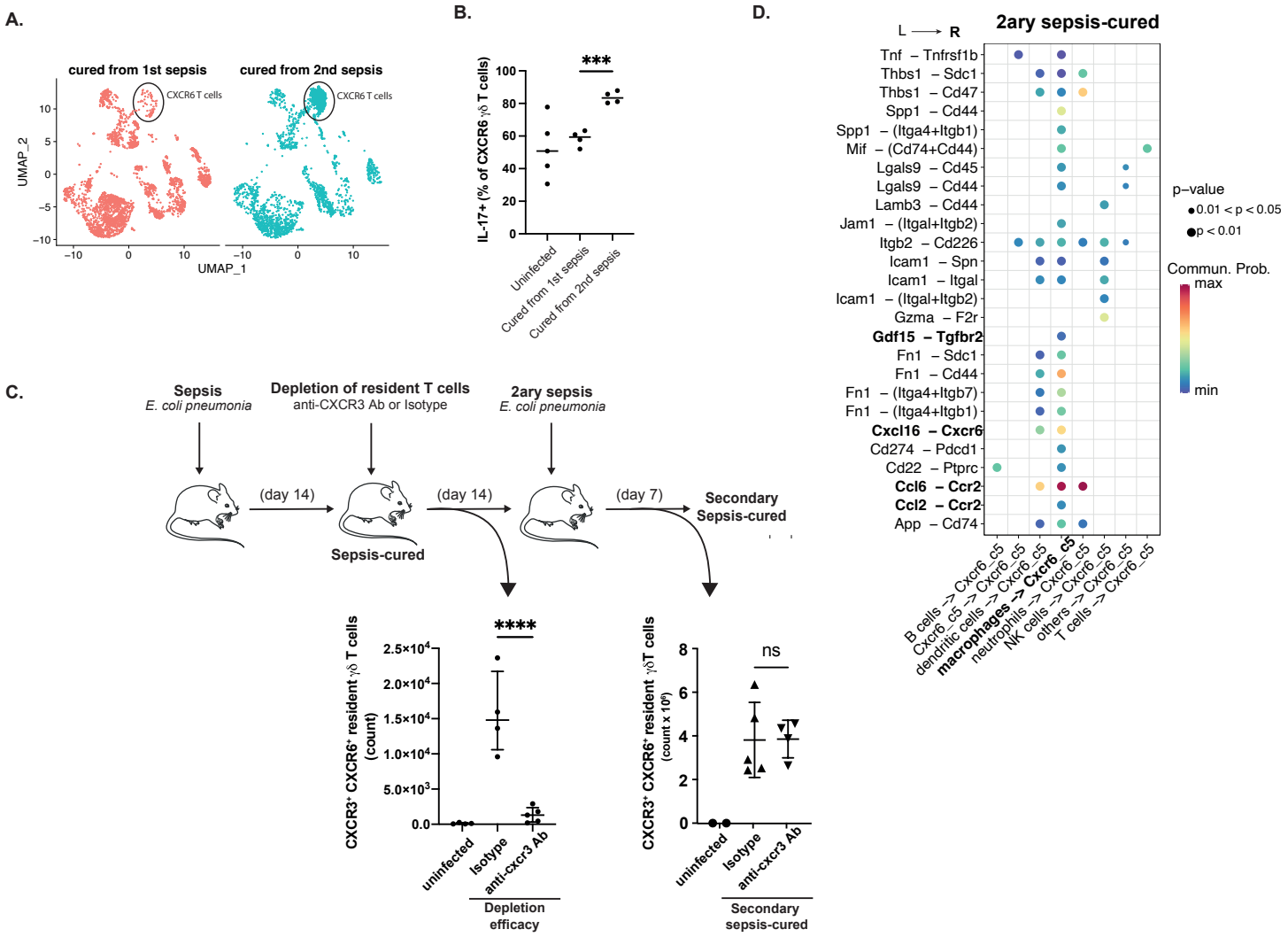

Figure S8

A. UMAP represents the cell distribution in primary (left panel) and secondary (right panel) sepsis. To be able to compare UMAPs, 800 cells were randomly selected in both conditions.

B. Percentages of IL17+ cells among resident CXCR6+ γδT cells (n= 4-5 mice/group). Graphs represent median ± IQR and are pooled data from 2 independent experiments.

C. Mice were infected with E. coli; 14 d later, the mice were treated with anti-CXCR3 or isotype control and were finally assessed 7 days after the induction of secondary lung sepsis. (Top) Experimental design. (Bottom left) Enumeration of CXCR3 CXCR6 resident γδ T cells before the induction of secondary sepsis. (Bottom right) and after the cure of secondary sepsis. (n=4 / group). Graphs represent median ± interquartile range and are pooled data from 2 independent experiments.

D. R-L map in the lung after secondary sepsis. Communication probability between CXCR6 T cells expressing receptors (R) and other cell types expressing cognate ligands (L). Both receptors and ligands were expressed in a minimum of 5 cells, and the curated lists of mouse-specific receptors and ligands were provided by the R package CellChat. Communication probabilities with p-value < 0.05 were considered significant. Statistical significance was assessed.

One-way analysis of variance with Bonferroni correction was used for multiple comparisons (B-C).
*P ≤ 0.05, **P ≤ 0.01, ***p<0.001.

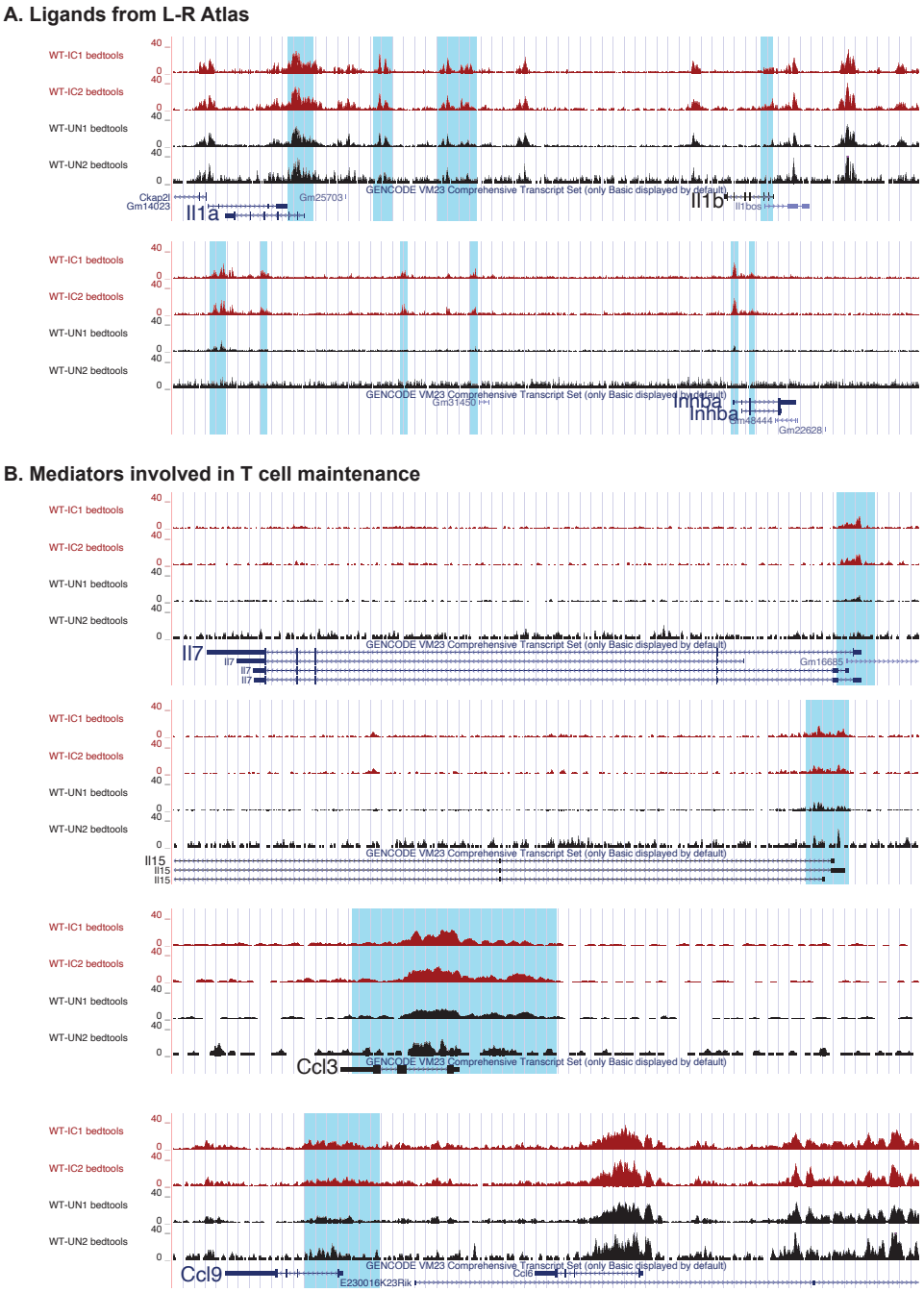

Figure S9

A. Promoter and enhancer activity at Il1b and Inhba loci, both genes of the TFG family, in resident alveolar macrophages before (black) and after (red) sepsis.

B. Promoter and enhancer activity at Il7, Ccl3, and Ccl9 loci in resident alveolar macrophages before (black) and after (red) sepsis.

A.

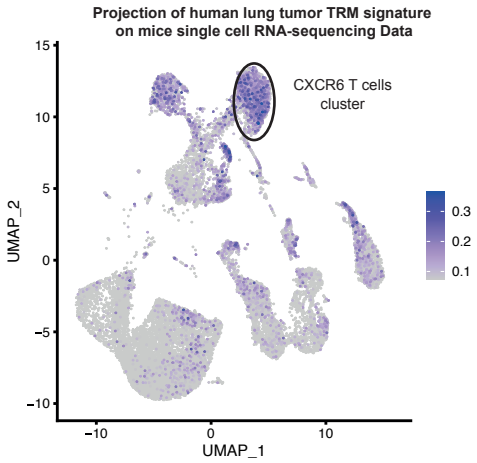

B.

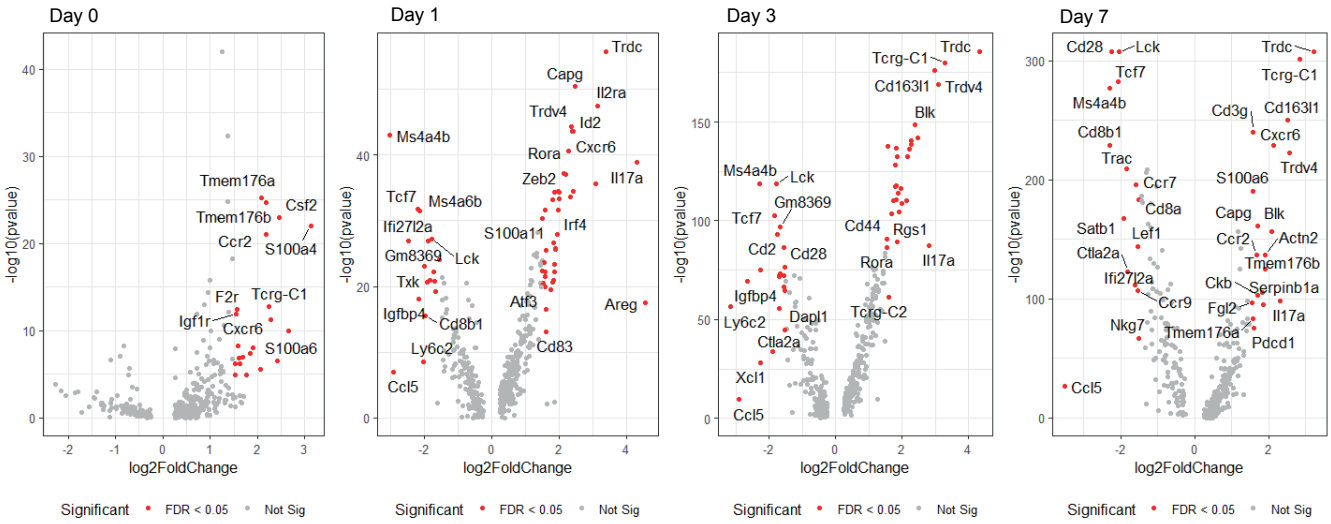

Actn2, Aqp3, Atp2b4, Blk, Camk2n1, Capg, Ccr2, Cd163l1, Cdkn1a, Ckb, Cxcr6, F2r, Il2ra, Lgals1, Lmna, Ltb4r1, Maf, Ramp1, Rora, S100a10, S100a11, S100a4, S100a6, Scpep1, Sdc4, Serpinb1a, Tcrg-C1, Tmem176a, Tmem176b, Trdc, Trgv2, Vim, Zeb2

Figure S10

A. Projection of the gene signature of human dermis tissue-resident T cells (from GSE83637) on the UMAP representation of sc-RNA-seq of lung tissue from septic-cured mice.

B. Definition of a CXCR6 tissue-resident T cells signature in sepsis-cured mice.

Visual abstract

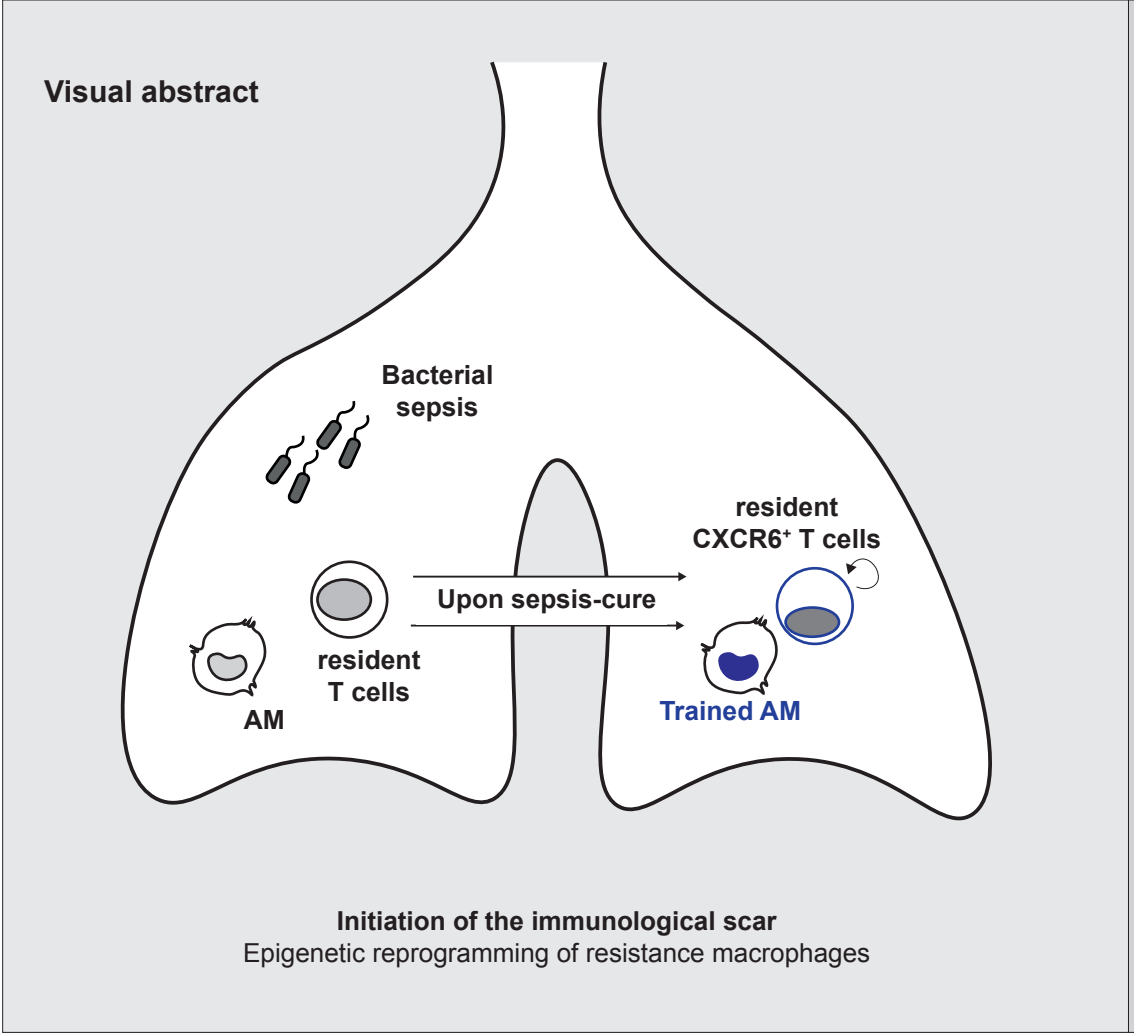

Initiation of the immunological scar
Epigenetic reprogramming of resistance macrophages

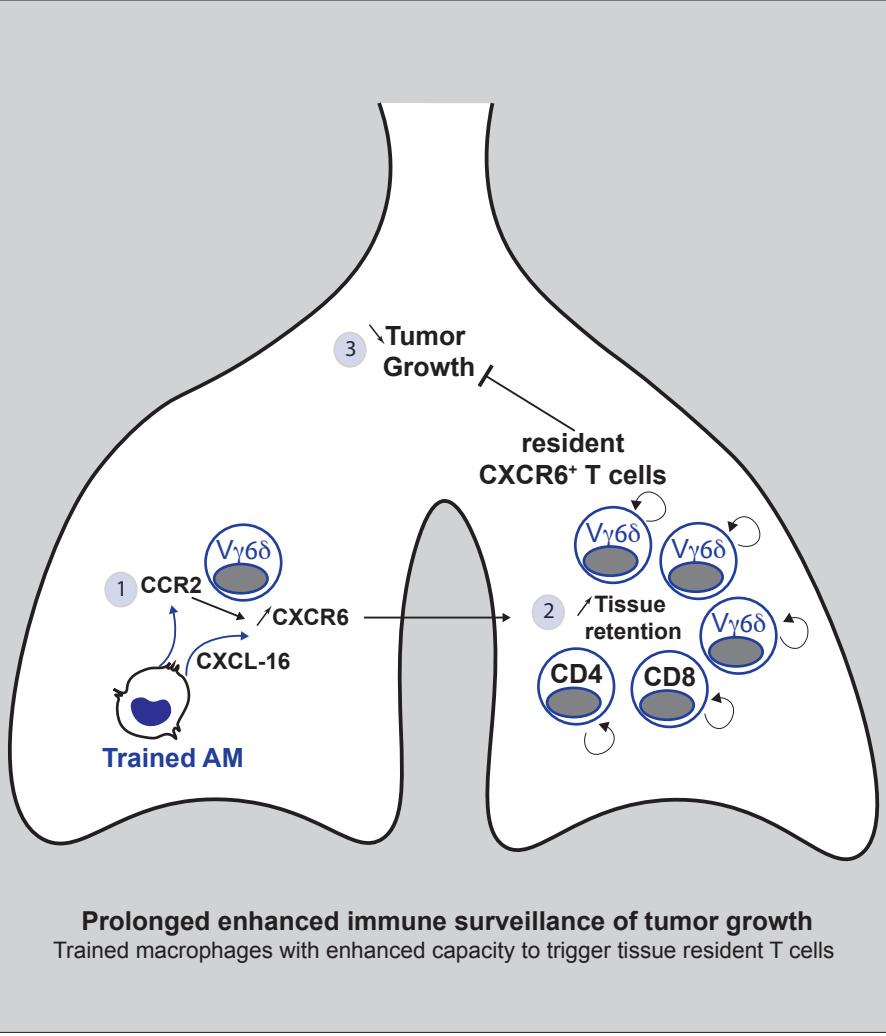

Prolonged enhanced immune surveillance of tumor growth
Trained macrophages with enhanced capacity to trigger tissue resident T cells

Cure from extracellular bacterial sepsis (for instance, Escherichia coli or Staphylococcus aureus) is associated with the formation of epigenetically reprogrammed macrophages (trained) and local accumulation of CXCR6 tissue-resident T cells.
Upon immune restimulation during cancer growth, trained macrophages release a cytokine and chemokine network that (1) increases the expression of CXCR6 by T cells via CCR2 stimulation and (2) sustains tissue residency of CXCR6 T cells via the production of CXCL16. (3) Locally expanded CXCR6 tissue-resident T cells, mainly composed of IL17+ RORγt+ Vγ6δ T cells, reduce tumoral growth.

Table S1. Demographic characteristics (Crude samples)

	Cohort 1 - Sepsis effect		Cohort 2 - SIRS effect		
	Sepsis	**Infection**	**Non-septic SIRS**	**No SIRS**	**Missing Values (%)**
n	66680	614923	89561	3040048	
Cause of hospitalisation, no (%)					0
Limb/pelvis trauma	23852 (35.8)	169512 (27.6)	57614 (64.3)	2126633 (70.0)	
Brain injury	3925 (5.9)	15882 (2.6)	8567 (9.6)	205489 (6.8)	
pneumonia	22192 (33.3)	429299 (69.8)	0 (0.0)	0 (0.0)	
stroke	16711 (25.1)	230 (0.0)	23380 (26.1)	707926 (23.3)	
Intensive care, yes, no (%)	66680 (100.0)	0 (0.0)	89561 (100.0)	0 (0.0)	0
Hospitalization, days, mean (SD)	24.00 [13.00, 41.00]	7.00 [4.00, 12.00]	12.00 [7.00, 21.00]	4.00 [2.00, 9.00]	0
Age, years, mean (SD)	57.67 (18.06)	70.97 (19.14)	49.10 (19.32)	61.29 (21.83)	0
Male, no (%)	41190 (61.8)	256899 (41.8)	60950 (68.1)	1529125 (50.3)	0
Medical history, yes, no (%)					
Infection	11976 (18.0)	111067 (18.1)	0 (0.0)	0 (0.0)	0
Cardiovascular diseases	8322 (12.5)	79944 (13.0)	6256 (7.0)	89902 (3.0)	0
Alcohol	15653 (23.5)	54178 (8.8)	13779 (15.4)	185209 (6.1)	0
Obesity	15957 (23.9)	104280 (17.0)	12265 (13.7)	244635 (8.0)	0
Socio-economical in the living area [IQR]					
% working population without high degree diploma	49.75 [38.33, 61.25]	52.25 [40.50, 64.00]	47.75 [36.75, 60.00]	50.50 [39.25, 62.25]	0
% mono-parental family	14.25 [11.00, 18.12]	13.50 [10.62, 17.50]	14.12 [10.88, 18.12]	13.62 [10.62, 17.62]	0
Unemployment rate	12.50 [9.75, 16.12]	12.38 [9.75, 15.75]	12.12 [9.50, 15.38]	12.25 [9.62, 15.75]	0
% unspecialized workers	23.25 [17.71, 29.12]	24.50 [19.00, 30.00]	22.62 [16.88, 28.50]	23.71 [18.25, 29.43]	0
		Outcomes at 9 years			
Cancer, nº (%)	6384 (9.6)	65285 (10.6)	6096 (6.8)	186373 (6.1)	0
Time to cancer, years, mean [IQR]	3.3 [2.0, 4.9]	3.0 [1.9, 4.7]	3.6 [2.2, 5.4]	3.5 [2.1, 5.2]	93,1
Death, nº (%)	9788 (14.7)	108239 (17.6)	5319 (5.9)	175555 (5.8)	0
Time to death, years, mean [IQR])	3.1 [1.7, 4.8]	3.0 [1.7, 4.7]	3.6 [2.0, 5.4]	3.5 [2.0, 5.3]	92,2

Table S2. Demographic characteristics (Matched samples)

	Cohort 1 - Sepsis effect				Cohort 2 - SIRS effect				
	Sepsis	**Infection**	**P**	**SMD**	**Non-septic SIRS**	**No SIRS**	**p**	**SMD**	**Missing Values (%)**
n	55,234	55,234			87,164	87,164			
Cause of hospitalisation, no (%)							<0.001	0.167	0
Limb/pelvis trauma	19,348 (35.0)	12,896 (23.3)	<0.0001	1.008	55,912 (64.2)	61,866 (71.0)			
Traumatic brain injury	3,096 (5.6)	1,472 (2.7)			8,384 (9.6)	8,442 (9.7)			
Pneumonia	19,550 (35.4)	40,797 (73.9)			-	-			
Stroke	13,240 (24.0)	69 (0.1)			22,868 (26.2)	16,856 (19.3)			
Intensive care, yes, no (%)	55,234 (100.0)	0 (0.0)	-	-	87,164 (100.0)	0 (0.0)	-	-	0
Hospitalization, days, mean (SD)	23.00 [13.00, 41.00]	6.00 [3.00, 11.00]	<0.0001	0.915	12.00 [7.00, 21.00]	3.00 [1.00, 7.00]	<0.001	0,771	0
Age, years, mean (SD)	59 (18)	59 (18)	0.0110	0.015	49 (19)	49 (19)	0.2708	0,005	0
Male, no (%)	33,838 (61.3)	31,466 (57.0)	<0.0001	0.087	59,336 (68.1)	59,129 (67.8)	0.2915	0,005	0
Medical history, yes, no (%)									
Infection	10,046 (18.2)	10,494 (19.0)	0.0010	0.021	-	-	-	-	0
Cardiovascular diseases	7,065 (12.8)	5,935 (10.7)	<0.0001	0.064	5,856 (6.7)	2,784 (3.2)	<0.001	0,163	0
Alcohol	13,109 (23.7)	10,003 (18.1)	<0.0001	0.139	13,507 (15.5)	11,385 (13.1)	<0.001	0,072	0
Obesity	13,385 (24.2)	11,586 (21.0)	<0.0001	0.078	11,879 (13.6)	10,214 (11.7)	<0.001	0,057	0
Socio-economical in the living area [IQR]									
% non-graduated people	47.75 [37.25, 59.50]	47.75 [37.00, 59.50]	0.6730	0.002	47.25 [36.50, 59.50]	47.25 [36.50, 59.80]	0.6748	0,002	0
% mono-parental family	14.38 [11.00, 18.43]	14.50 [11.12, 18.50]	0.0062	0.017	14.12 [10.88, 18.12]	14.12 [10.97, 18.40]	0.0314	0,010	0
% unemployed people	12.29 [9.62, 15.88]	12.38 [9.62, 15.88]	0.4770	0.003	12.12 [9.50, 15.38]	12.12 [9.50, 15.40]	0.7824	0,002	0
% workers	22.75 [17.00, 28.50]	22.71 [17.00, 28.50]	0.0938	0.009	22.50 [16.88, 28.43]	22.50 [16.90, 28.50]	0.2996	0,006	0
Outcomes at 9 years									
Cancer, no (%)	5,473 (9.9)	6,126 (11.1)	<0.0001	0.039	5,916 (6.8)	4,905 (5.6)	<0.001	0,048	0
Time to cancer, years, mean [IQR]	3.3 [2.0, 4.9]	3.3 [2.0, 5.0]	0.4071	0.008	3.6 [2.2, 5.4]	3.5 [2.2, 5.2]	0.2947	0,024	92,5
Death, no (%)	8,496 (15.4)	7,125 (12.9)	<0.0001	0.071	5,160 (5.9)	3,576 (4.1)	<0.001	0,083	0
Time to death, years, mean [IQR]	3.1 [1.7, 4.8]	3.3 [1.9, 5.0]	<0.0001	0.087	3.6 [2.1, 5.4]	3.7 [2.2, 5.6]	0.0032	0,062	92,1

!"#$%&'"()* %

%

%

(+&#,%#,"-.)*-'! %

!

/01 % 2340 2045/6778 592958/: :30/8% ;634<60 670<=> 30% $$-* %

"#$! %&% ()*(+ ! (),,-./ ! "#$ 01 ! ,21-- ! 3(4!5671, 78$1.9$9/ 0$! :;<1../,/ !

"#,.=!

>"?"8=@ %&% A&BCD!;E&F&6 AGH,,-1! I&FJ*F&% ,21-- ! 3())E4!567 =K=± :;<,----/L, !

! ! ! ! ! ! ! ! !

%

&-?' %,"-.)*-'! %

%&+	MFC&	M&C3%ED'(	3NMN3'%*'	*F&%'	OEFC4E&%	ED&4J'	F&4	885#	:II
""G1!	%&%'	;E&G'6'%O	L-L/,$!	1PL!	,--C62+&CD'!	(3+!Q(+D4'3	;1//$K, !	:;<1.1--.. !	
"#,/1!>""81@!	ST!	)E&F'6'%O	,L-=,- !	H:1-$7,, !	,21-- !	3(4!5671)UV	;1$L,1K !	:;<1=,=/.1 !	
"#,-$!	BE&)3E6Q4	+EF4'%JE!;E&4	,$- 0,, 0=.9 !	8T:9./ !	,2,-- !	QC+(%!567,	!	:;<19.$.//	
"#,,) !	)B=-L!	;E&G'6'%O	,-,1L9 !	W,29-!	,21-- !	3(4!5671)UV	;$,=..- !	:;<1L=LK$, !	
"#,,* !	S"'J9 !	;E&G'6'%O	,,9$,. !	AK,. !	,21-- !	Q(+D4'3!567,UV	;1/-,L1 !	:;<K/$L=. !	
"#1K!	)B9,, !	;# !	L=$KL!	W,2=/!	,21-- !	3(4!5671)UV	,,$./$!	:;<19$.1,$!	
"#$!	)B9,, !	;# !	L=$,1$!	,KL01",, !	,21-- !	Q(+D4'3!567,UV	9$,,L/9 !	:;<1=.9/LK !	
"#K!	(F'X(MFC&3!K	;# !	LL9==9	8WK0L!	,21-- !	3(45671(UV	K,$$/K- !	:;<$/=99/ !	
"#K!	;YZ$/L !	;# !	L=$9/- !	7[,\L !	,21-- !	3(4!5671)UV	,-/99$K !	:;<19$.K1= !	
"#KK!	)BK.- !	;# !	L==,,= !	5W9	,21-- !	3(4!5671)UV	.1199L1!	:;<19$/L,. !	
"#KL!	ST!	)E&F'6'%O	,-$,-= !	$-0R,, !	,21-- !	3(4!5671)UV	;1/K9K1!	:;<$,1/9, !	
"#KL!	)BK.- !	;# !	L==-/L !	$-0R,, !	,21-- !	3(4!5671)UV	9,KKL-=!	:;<19$/L=L !	
"#KL\, !	S"'J9 !	;# !	L=-L9. !	:1- !	,21-- !	3(4!5671(UV	.,19.,. !	:;<,919K.. !	
"#KL\1!	S'3"S0'JL\L!	;# !	LL1/L- !	,-K !	,21-- !	3(4!5671(UV	.,L1.// !	:;<$/KL1. !	
"#=/ !	:S" !	;# !	L=-=./ !	P,\1R$	,21-- !	Q(+D4'3!567	/1-K919!	:;<,919L-= !	

"#.! !	(F'X(MFC&3!9	;# !	LL9/L/ !	8S:0. !	,21-- !	3(4!5671(UV	/-1L9KL!	:;<$/=/L/ !
"?"G,=!	ST!	;# !	L==9K!	1//1, !	,2,-- !	3(4!567,UV	$L---$!	:;<1.=/.K1 !
"?"G,=!	%&%''	8^# !	W:;L-$ 0L-- !	,K1K,9!	L-C62+&CD'	3(4!5671(	RP_-1,9,,, !	:;<119=9L1!
"#,.$! >"?"8$@	%&%''	;E&G'6'%D	,1=L$9!	"?"8$ 09$!	1--C6!2!,--C6!EE	(3+!Q(+D4'3!567,V	;1/1$,K !	:;<1L9,/// !
"#,.=!>"?"8=@!	ST!	)E&F'6'%D	,L,,-K !	H:-L,#, !	,21-- !	3(4!5671)UV	;1/,/9, !	:;<1L==LK=!
"#,.=!>"?"8=@!	ST!O(``F'!L/K	;E&G'6'%D	,L,,,= !	H:-L,#, !	,2,-- !	3(45671)UV	;1==K1/!	:;<191,9-- !
RK2.!	(F'X(MFC&3=	;E&G'6'%D	,1$,,- !	;W. !	,21-- !	3(4!5671(UV	;$K.,9L !	:;<./$K.- !
7(4($!	)BK1,!	;# !	L=$$K!	GL01$!	,2,-- !	+&CD'!567,UV	9,$,/=- !	:;<19$.,L1 !
5RA6	(F'X(MFC&3K	;# !	LL991K	?W7,\1!	,2,-- !	3(4!567,UV	!	:;<$/=.$1 !
5RA6	ST!	;# !	LLKK,1!	?W7,\1!	,2,-- !	3(4!567,UV	.1$LL=L!	:;<$/L$9= !
5G9: !	ST!	4Q'3+&MED!Q'	,1 09,990, !	';E&,9;9 !	,2,-- !	3(4!5671(UV	K19=/,K!	!:;<9=$L.1
				;Z#K 0				
5GK!	ST!	;# !	LLK$./!	,#,, !	,2,-- !	3(4!5671)	9,.-/,- !	:;<$/L$=, !
VE=9	)BK1,!	;# !	L=1.// !	;L=!	,2,-- !	+&CD'!567,UV	.1/==,9 !	:;<1=.=./9 !
W8,!	!	!	!	!	!	!	!	!
A[,\, !	)BK1,!	;# !	L=1/1,!	S[,$=!	,21-- !	+&CD'!5671(UV	9,=L9!	:;<191.=.. !
A[,\, !	ST!	;# !	LL$,=L!	S[,$=!	,21-- !	+&CD'!5671(UV	9-=/.$K !	:;<$/==9K !
8a864	)BK1,!	;# !	L=1./K!	b$, 0$9.!	,2,-- !	+&CD'!5671(UV	.,L,.=, !	:;<1=.9LKL !
4)'4 !	)BK1,!	;# !	L=$$,.!	aK0K=!	,2,-- !	+&CD'!567,UV	.19LL/, !	:;<1=.9LK$!
]"8!)'4(!	S'"J9 !	)E&F'6'%D	,-/111 !	PL90L/9!	,21-- !	Q(+D4'3!567	;1=.1L/ !	:;<./$=1L !
]"8!6O!	S'0'J9!	)E&F'6'%D	,,.,1$!	7G$	,21-- !	Q(+D4'3!567	;1/,KK=!	:;<,,1-KK1$!
]AR(!	ST!	;# !	LLKK,/!	WS=0?]11!	,2,-- !	3(4!567!,	K1$$=K!1	KK$=$
]"8!Z6,\,2"3K !	R5]"!	;E&G'6'%D	,K,,-K !	1\,, !	,21-- !	(3+!Q(+D4'3	;1=.9./ !	:;<,-=/9-$, !
]"8!Z61!>Z6K!@	ST!	;E&G'6'%D	,$99-=!	Y"T0,-:= !	,21-- !	(3+!Q(+D4'3	;1./L$. !	]"8!Z61!>Z6K!(
]"8!Z6=!	%&%''	_\!_&DQE=V(E	%&%''	5",- 05R9	,21-- !	+&CD'!567,UV	!	Q&+'0+(O' !

!

!

)"('$ %

/01 %	234	2045/6778	592958/:8	:30/8%	;634<60	670<=>
MEX()F'!BE()EFE	4J!OJ'	'MFC&39	4Q'3+&MED	Q'3	=L0.=L 0	K!	%2(	,2,--- !	%2(
+&CD'!576!		ST!	4Q'3+&MED	Q'3	,1 0K9,K0	K1!	S$\=\1\.\,!	,2,-- !	+&CD'!576!
+&CD'!5671(U	V	)BK1,!	;# !		L=1K$/!		7,LL 0	9. !	,2,-- !	+&CD'!5671(U	V
3(4!5671(U	V	ST!	4Q'3+&MED	Q'3	,1 0K$1,0	, !	';81(!	,2,-- !	3(4!5671(U	V
3(4!5671(U	!V	%&%'	4Q'3+&MED	Q'3	,= 0K$1,0	L !	';81(!	L-C62D&C3E	3(4!5671(U	!V
!		!	!		!		!	!	!	
D43'I4(BEC	E%!	ST!	;# !		LLK-=,!		!	!	!	
!		!	!		!		!	!	!	
"I7!a#A,==. !		!	5%BEB&6'%		4F0	=. !	!	1-%W	!	
					A;S10$L,==0					
+"?"G,=!3'*&+) !		!	A&BCD	&F&6E*(F	1LC6		!	!	!	
&B(F)C+E%		!	HE6+(		:9=K, !		!	1--C6!>E\4\@	!	
%(EB'!"#.(!]!*'FF!ED&F(4E&%!'										
+&CD!		!	+EF4'%JE		,$- 0	/= 0LK$	!	!	!	
!		!	!		!		!	!	!	
#&%V'J!(%4E!+&C	D'!	(F'X(MFC&3	K9	5%BE43&6'%	:$,L9, !		!	,2L-- !	O&%V!J	
O&%V'J!(%4E!3(4		(F'X(FC&3K	.	5%BE43&6'%	:1,1-. !		!	!	O&%V!J	
O&%V'J!(%4E	E)E4	(F'X(MFC&3L	=.	5%BE43&6'%	:,--K1 !		!	!	O&%V!J	
+&C%4E%6!+'OE	EC+	!		5%BE43&6'%	S$=/=1!		!	!	!	
				TF'*43&%E	E*3&D*&IJ!					
I(3(M&3+(FO'QJ	'	!	H*E'%*'D		,L9,K !		!	!	!	
]3E4&%!	? !	!	HE6+(!:FO3E	*Q	]/1.K 0	--WG !	!	!	!	
!		!	!		!		!	!	!	
									(3+!Q(+D4'3!	
(3+'%E(%!Q(+D4'3!56	7,	%&%%	;E&G'6'%	D	K--/L/ !		P][... !	1--C62,--C6 !	567,!	
3())E4!56	7	%&%%	)E&4'*Q%	'	:; 0-L 0	' !	!	,21-- !	3())E4!56	7
3(4!567	!,	%&%%	)E&4'*Q%	'	W:;--L !		K$K,K	,21-- !	3(4!567	!,

!	!	!	!	!	!	!
;=\,1/S1 0"X*3=4+,GE4!42c	!	]Q'!c(*VD&%!G()&3(4!&3	L=/$!	!	!	!
;=\,1/HK 0"*314+,5M*!2c	!	]Q'!c(*VD&%!G()&3(4!&3	K/// !	!	!	!
;=\,1/H9 05M%63,4+,:64!2c	(!*&%ME3+'3!I(3! "#]: !	]Q'!c(*VD&%!G()&3(4!&3	$1.. !	!	!	!
;=\Hc0G54I3*(S'I*)2;&J"3F!	!	"Q(3F'D!8EB'3	K/K!	!	!	!

%